Recent Advances in Electrochemiluminescence with Quantum Dots and Arrays of Nanoelectrodes

Paolo Bertoncello[a] and Paolo Ugo[b]

[a]College of Engineering, Swansea University, Bay Campus, Swansea SA1 8EN, United Kingdom

[b]Department of Molecular Sciences and Nanosystems, University Ca' Foscari Venice, via Torino 155, 30175 Venezia-Mestre, Italy

Abstract

This review presents the last advances related to analytical and bioanalytical applications of electrochemiluminescence (ECL) achieved by exploiting the special optical or electrochemical properties of quantum dots and nanoelectrodes, respectively. After a brief introduction which covers the basic concepts of ECL detection, the review presents relevant examples dealing with in the use of quantum dots and arrays of nanoelectrodes to improve the analytical and bioanalytical capabilities of ECL. Finally, prospects and limits derived from the application of the above advanced nanomaterials to stimulate ECL emission are discussed.

Keywords

Electrochemiluminescence; quantum dots; nanoelectrodes; array; electrochemical sensors

Introduction

Electrochemiluminescence (ECL) or electrogenerated chemiluminescence is an analytical technique in which electrochemically generated intermediates undergo electron-transfer reactions to form electronically excited states that emit light[1], [2], [3], [4]. The first detailed investigations about ECL were reported by Hercules[5], and Bard[6] in the early 1960's, even though seminal studies regarding light emission under electrolysis conditions were reported earlier by Harvey in the 1920's[7]. As a form of luminescence (e.g. emission of light without heat), and in contrast to chemiluminescence (CL) where light emission is the result of a chemical reactions between suitable species, ECL has the peculiarity that light emission occurs when a suitable potential (oxidation or reduction) is applied at the electrode[3]. As such, ECL has several advantages over CL, in particular, the electrochemical reaction allows the time and position of the light-emitting reaction to be carefully controlled; control over the time means the light emission can be delayed until specific events such as immune or enzyme-catalysed reactions have taken place; control over position can be used to confine the light emission into a precisely located region with respect to the detector. These advantages lead to enhanced sensitivity by increasing the ratio of signal to noise. ECL occurs by means of two distinct processes: (i) ion annihilation and (ii) coreactant ECL. Ion annihilation involved the formation of excited states as a result of exergonic electron-transfer between electrochemically generated species (typically radical ions) at the surface of electrodes. Let us consider a luminophore (emitter) species, *R*, which is oxidised and reduced at the electrode. The ion annihilation ECL occurs through the following steps:

$R - e^- \rightarrow R^{+\cdot}$ (oxidation) (1)

$R + e^- \rightarrow R^{-\cdot}$(reduction) (2)

$R^{+\cdot} + R^{-\cdot} \rightarrow R + R^*$ (excited state formation) (3)

$R^* \rightarrow R + h\upsilon$ (light emission) (4)

Annihilation occurs in Eq. 3 with the formation of the excited species, *R**. Annihilation reactions can also occur with different species, *i.e.* when the radical cation and anion derive from different molecules. For ECL co-reactant, let us consider *R* and *C* as the emitter and coreactant species, respectively. Typically, coreactant ECL is generated by applying an anodic or cathodic potential in a solution containing the luminophore and the coreactant. Therefore, depending on the polarity of the applied potential, both luminophore and coreactant species can be oxidised or reduced at the electrode to form radical ions, and

intermediates species followed by decomposition of these species and formation of excited states that emit light. Because highly reducing intermediate species are generated after electrochemical oxidation of coreactant or highly oxidising intermediates are produced after electrochemical reduction, the corresponding ECL reactions are often defined as "oxidative-reduction" for the former and "reductive-oxidation" ECL for the latter, respectively. Use of coreactant is useful in chemical analysis when one of the $R^{\bullet+}$ or $R^{\bullet-}$ is not stable enough for ECL reaction, or in the case the solvent being used has a narrow potential window so that $R^{\bullet+}$ or $R^{\bullet-}$ cannot be formed. When the annihilation reaction between oxidized and reduced species is not efficient, the use of a coreactant may produce more intense ECL. To mention also an additional advantage, *i.e.* the quenching effect due to molecular oxygen, which is significant in ion annihilation ECL, may be eliminated during "oxidative-reduction"-type ECL, thus the experiment can be conducted in air. The mechanism for coreactant ECL can be generalised as follows. Case (a) oxidative-reduction co-reactant ECL:

$$R - e^- \rightarrow R^{+\cdot} \quad (5)$$

$$C - e^- \rightarrow C^{+\cdot} \quad (6)$$

$$R^{+\cdot} + C \rightarrow R + C^{+\cdot} \quad (7)$$

$$C^{+\cdot} \rightarrow C_{red}^{\#} \quad (8)$$

$$C_{red}^{\#} + R \rightarrow R^{\cdot -} + P \quad (9)$$

$$R^{\cdot -} + R^{+\cdot} \rightarrow R + R^* \text{ or } R^{+\cdot} + C_{red}^{\#} \rightarrow R^* + P \quad (10)$$

$$R^* \rightarrow R + h\upsilon \quad (11)$$

Case (b) reductive-oxidation co-reactant ECL:

$$R + e^- \rightarrow R^{-\cdot} \quad (12)$$

$$C + e^- \rightarrow C^{-\cdot} \quad (13)$$

$$R^{-\cdot} + C \rightarrow R + C^{-\cdot} \quad (14)$$

$$C^{-\cdot} \rightarrow C_{ox}^{\#} \quad (15)$$

$$C_{ox}^{\#} + R \rightarrow R^{+\cdot} + P \quad (16)$$

$$R^{\cdot -} + R^{+\cdot} \rightarrow R + R^* \text{ or } R^{-\cdot} + C_{ox}^{\#} \rightarrow R^* + P \quad (17)$$

$$R^* \rightarrow R + h\upsilon \quad (18)$$

where (5), (6), (12), and (13) represent the redox reactions at the electrode, (7), (8), (9), (14), (15), and (16) are homogenous chemical reactions, (10), and (17) the excited state formation species, (11), and (18) the light emission, with *R* representing the emitter, *C* the co-reactant,

$C_{red}^{\#}$ and $C_{ox}^{\#}$ are the coreactant intermediates for the reducing and oxidising agents, respectively, and P the products associated with $C^{\#}$ reactions. The most common luminophore used in coreactant ECL is $Ru(bpy)_3^{2+}$, while tripropylamine (TPrA), oxalate, perdisulfate ions and hydrogen peroxide are the most popular coreactant species[3].

Many recent devolopments in the study and applications of ECL are related to the new prospects opened by the use of novel nanomaterials and electrodes of nanometric size[8], [9], [10], [11], [12]. . The downsizing of the components of the ECL generation/detection system allows indeed to exploit some special characteristics observed in materials with critical dimension in the few nanometers range. Among the large variety of nanomaterials today available, we choose to focus our review on ECL phenomena which exploit the special properties of inorganic semiconductor quantum dots and of arrays nanotube/nanodisk electrodes, where the control of the size and spatial distribution of the nanocomponents plays a well defined role, bringing to increase in ECL emission because of quantum or molecular diffusion effects. For reasons of space, the readers interested on recent advances in ECL based on different nanomaterials, such as graphene and carbon quantum dots, can refer to other specific reviews[13], [14], [15]. Note also that this review focuses on, but is not limited to, papers published in the last five years.

ECL of quantum dots

Semiconducting nanocrystals or quantum dots (QDs) are a class of nanomaterials with unique optoelectronic properties that have found a variety of applications, from energy conversion systems to electronics and diagnostics[16]. The physical properties of QDs are essentially dictated by quantum confinement effects and are considerable different from their analogous as bulk materials. To summarise this concept using the band theory, when photons are used to excite QDs with energy equal or greater than their band gap, then the resulting effect is the excitation of electrons from the valence to the conduction band with concomitant formation of a hole in the valence band. The formation of such electron-hole (*e*-*h*) pair ("exciton") is bound by electrostatic attraction with the opposite charges and the extension of the exciton wave function over the crystal lattice is measured by the Bohr radius[11]. In simpler words, the Bohr radius is a measure of the average distance between the holes and the photo-generated electrons. A typical example is the case of CdSe QDs, where the Bohr radius is about 6 nm. When CdSe QDs have size smaller than the Bohr radius, then the optical and electrical properties become dependent on its physical dimensions, owing to quantum confinement

effect. When this situation occurs, the band structure of QDs changes into discrete levels and the difference in the energy levels between HOMO and LUMO widens as the size particle decreases. However, a description based on the molecular orbits rather than on the band theories is quite often more appropriate to describe QDs as a system lying between bulk materials and molecular species. The process of charge transfer within QDs can be summarised as in Figure 1.[17] The energy required to produce a non-interacting *e-h* pair is defined as a quasi-particle gap, which in fact corresponds to the electrochemical band gap, *i.e* the difference between the first oxidation and first reduction of QDs. The electrochemical band gap, ΔE_{el} can be determined voltammetrically (Figure 1c), instead the optical band gap, ΔE_{opt} (Figure 1d) can be quantified using spectroscopic data. ΔE_{el} and ΔE_{opt} are correlated by the expression:

$$\Delta E_{opt} = \Delta E_{el} - J_{e,h} \qquad (19)$$

Where $J_{e,h}$ is the total Coulombic energy of the *e-h* pair. Eq. 19 implies that the electrochemical band gap is larger than the optical energy gap. Therefore, voltammetric methods are very useful to estimate HOMO-LUMO levels in electroactive species, as well as to determine parameters such as electron transfer kinetics, diffusion coefficients and kinetic constants. More importantly, while with spectroscopic methods it is possible to probe processes occurring inside QDs, instead with voltammetric methods it is possible to probe the QDs surface states that are inherently defective due to the presence of entangled bonds and unsaturated valences.

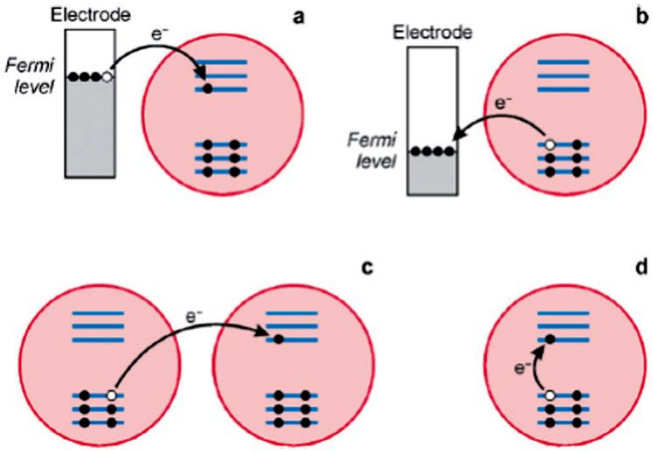

Figure 1. Schematic of mechanism of charge transfer in semiconducting QDs: (a) electron-transfer from a conductive electrode to neutral particle; (b) hole injection from electrode to QDs ("electron-extraction"); (c) simultaneous injection of electron and hole in two non-interacting QDs; (d) generation of electron-hole ("e-h") pair within the same QDs. Reprinted from Ref. [16] with permission of the Royal Society of Chemistry.

Since the initial discovery of QDs in 1983 from Brus *et al.* [18],[19], and breakthrough applications in bioanalysis from Alivisatos[20] and Nie[21], in the last decade the number of works related to QDs in chemical analysis has dramatically increased. The first seminal description of electrochemiluminescence from QDs was reported by Bard in 2002 and involved the ECL generation from germanium[22] and silicon[23] nanocrystals in DMF. Soon after, ECL works of functionalised CdSe[24], core-shell CdSe/ZnSe[25], and CdTe QDs[26] in organic solvents followed. However, a real breakthrough of ECL of QDs in bioanalysis is represented by the work of Liu *et al.* in which for the first time the synthesis of water soluble mercaptopropionic-capped CdTe and anodic ECL detection of cathecol derivatives was reported[27]. In QDs, the ECL processes involve the formation of high-energy electron transfer reactions with formation of excited species. From the formation of excited species, the emission of light occurs through two distinct mechanisms, (i) annihilation and (ii) coreactant ones. The annihilation pathway involved with QDs can be summarised as follows [10], [28]:

$$QD_s + e^- \rightarrow QD_s^{-\cdot} \quad (20)$$

$$QD_s - e^- \rightarrow QD_s^{+\cdot} \quad (21)$$

$$QD_s^{+\cdot} + QD_s^{-\cdot} \rightarrow QD_s + QD_s^* \quad (22)$$

$$QD_s^* \rightarrow QD_s + h\upsilon \quad (23)$$

The radical ions formed in Eq. 20 and 21 during the reduction and oxidation scans, respectively, are unstable and characterised by short life time. The reactions between the radical anions and cations leads to the formation of the excited species QDs* which emits light at the characteristic wavelength of the as-prepared QDs. Note that the annihilation pathway requires only the presence of the luminophore species (QDs), solvent and supporting electrolyte to generate light, however a major drawback is represented by the fact that in bioanalysis, the potential window of aqueous solution is often not wide enough to allow the formation of radical ions (cations and anions). In this case, organic solvents such as acetonitrile and *N,N*-dimethylformamide must be utilised, which is not practical for bioanalytical applications[4], [29]. Also, annihilation requires that the life-time of the

electrogenerated species must be long enough to react and to produce the excited species: obviously, this is an intrinsic limitation, especially if the electrogenerated species is prone to react with the solvent. This implies that in real samples the coreactant pathway is largely the predominant route utilised in ECL. In the coreactant pathway, co-reactant species are oxidised and reduced at the electrode surface, with the formation of radical cations or radical anions. These radical ions react with the oxidised or reduced formed of QDs leading to the formation of excited quantum dots, QDs*. The main difference with the annihilation pathway in which oxidised and reduced ECL species must be generated at the same time, is that coreactant ECL occurs by sweeping the electrode potential in one direction (anodic or cathodic) with the luminophore (QDs) reacting with radical ions from the coreactant species. The coreactant pathway is usually classified as (i) oxidative-reduction or (ii) reductive-oxidation as previously mentioned, and accordingly to the intermediate species generated during the anodic or cathodic potential sweep. Typical ECL coreactants belonging to the oxidative-reduction include TPrA, dibutylaminoethanol (DBAE), oxalate ($C_2O_4^{2-}$) and sulfite (SO_3^{2-}) species, while molecular oxygen (O_2), hydrogen peroxide (H_2O_2) and perdisulfate ($S_2O_8^{2-}$)[10], [30] are the most common coreactants belonging to the reductive-oxidation pathway. It is useful to recall the mechanism of reactions of QDs with TPrA and H_2O_2, which are the most common coreactant utilised in bioanalysis. For the oxidative-reduction pathway the mechanism of ECL generation is as follows[31], [32]:

$$TPrA - e^- \rightarrow TPrA^{+\cdot} \quad (24)$$

$$TPrA^{+\cdot} \rightarrow TPrA^{\cdot} + H^+ \quad (25)$$

$$QD_s - e^- \rightarrow QD_s^{+\cdot} \quad (26)$$

$$TPrA^{\cdot} + QD_s^{+\cdot} \rightarrow TPrA\ fragments + QD_s^* \quad (27)$$

$$QD_s^* \rightarrow QD_s + h\upsilon \quad (28)$$

In anodic ECL, the electrode first injects holes into the valence band of QDs with concomitant injection of electrons provided by the oxidation of the coreactant. Then, recombination of holes and electrons leads to anodic ECL. The process is summarised in Figure 2.

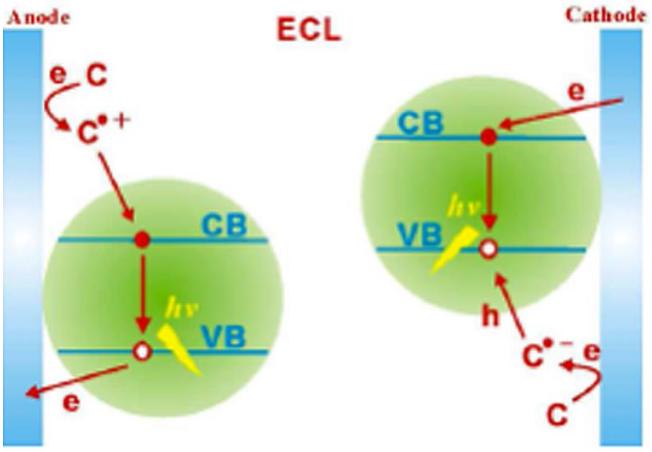

Figure 2. Anodic (A) and cathodic (B) ECL of QDs deposited on electrode surfaces in the presence of co-reactant speciess. Reprinted from Ref. [11] with permission of the American Chemical Society.

For the reductive-oxidation pathway, the ECL generation occurs as follows[33]:

$$H_2O_2 + e^- \rightarrow OH^- + OH^{\cdot} \quad (29)$$

$$QD_s + e^- \rightarrow QD_s^{-\cdot} \quad (30)$$

$$QD_s^{-\cdot} + OH^{\cdot} \rightarrow QD_s^* + OH^- \quad (31)$$

$$QD_s^* \rightarrow QD_s + h\upsilon \quad (32)$$

In this case, the role of the electrode and coreactant, and with them the role of holes and electrons are exchanged. Key advantages of the coreactant pathway is that the ECL generation is facilitated in aqueous solutions, opening up various and disparate possibilities for developing ECL-based essays for medical diagnostics[4]. ECL applications of QDs in bioanalysis coupled with the possibility of engineering their size, shape and composition at the nanoscale are opening up unprecedented opportunities. However, works related to ECL of QDs can be divided into four main streams: (i) synthesis of water compatible QDs, (ii) assembly of QDs on electrode surfaces, (iii) functionalisation and bioconjugation of QDs with biomolecules and chromophores, and (iv) integration of QDs-bioconjugated molecules into specific bioassays[11], [23],[34], [29] [35], [36], [37]. Herein, we focus on some of the most recent applications of QDs in bioanalysis.

Liu *et al.* developed a novel dual-stabiliser-capped synthetic strategy for preparing CdSe QDs for ECL detection of dopamine[38]. This synthetic strategy involves the immobilisation of marcaptopropionic-protected CdSe QDs on p-aminobenzoic acid modified glassy carbon electrodes and ethylenediamine as a link molecule. This procedure, summarised in Figure 3, allowed the synthesis of QDs with strong monochromatic ECL emission at 546 nm with

concomitant passivation of the QDs surface. In this way, non-radiative surface states and surface traps are removed, leading to high monochromaticity and highly efficient *e-h* injection.

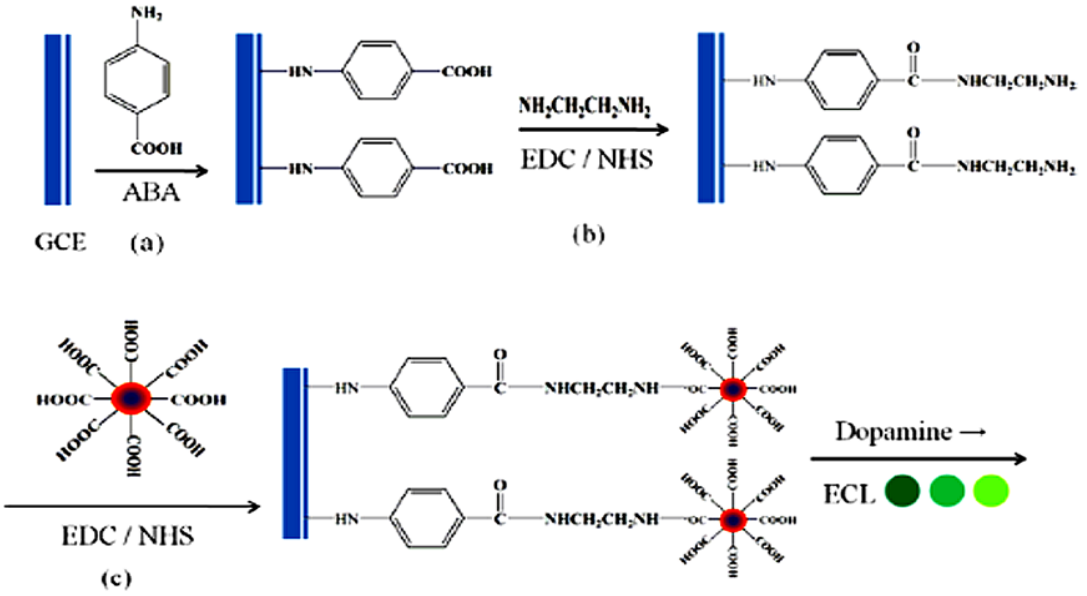

Fig. 3. Schematic of ECL configuration strategy. Reprinted from Ref. [38] with permission of the American Chemical Society.

The as-prepared ECL sensor allowed detection of dopamine in the linear range 10 nM – 3µM with a limit of detection of 3 nM without any signal amplification technique, by means of quenching of the ECL signal in the presence of $S_2O_8^{2-}$ as coreactant. While H_2O_2 is the most common coreactant for ECL in the cathodic region, only recently a detailed study from Russell *et al.* using a variety of coreactants has shown that $S_2O_8^{2-}$ is the most efficient among the coreactants[39]. The last five years have seen an explosion of ECL-based reports with a combination of a variety of nanomaterials, in particular gold nanoparticles (Au NPs)[36], silica nanoparticles (Si NPs)[40] and carbon nanomaterials (graphene, carbon QDs)[41], [42]. Such a combination of nanomaterials allows in principle the detection of the most disparate analytes in medical diagnostics. An interesting approach has been developed by Guo *et al.* for the simultaneous determination of two tumour markers, namely, alpha-fetoprotein (AFP), and carcinoembryonic antigen (CEA), using multicolour CdSe/ZnS QDs as labels and graphene as conducting bridge[43]. Two different sized CdSe/ZnS QDs were utilised to label secondary anti-AFP and anti-CEA antibodies. Such an approach allowed the production of two distinguished ECL signals at 525 nm and 625 nm without interference, with graphene acting as conducting bridge to promote electron transfer between QDs and the electrodes. A 30-fold

magnification of the ECL signal was evidenced in the presence of $S_2O_8^{2-}$ as co-reactant. A summary of the procedure utilised for the fabrication of the immunosensor is reported in Figure 4. This configuration enabled the simultaneous detection of AFP and CEA with a linear range of 0.001 – 0.1 pg/mL and detection limits for both analytes down to 0.4 fg/mL with no obvious cross-reactivity.

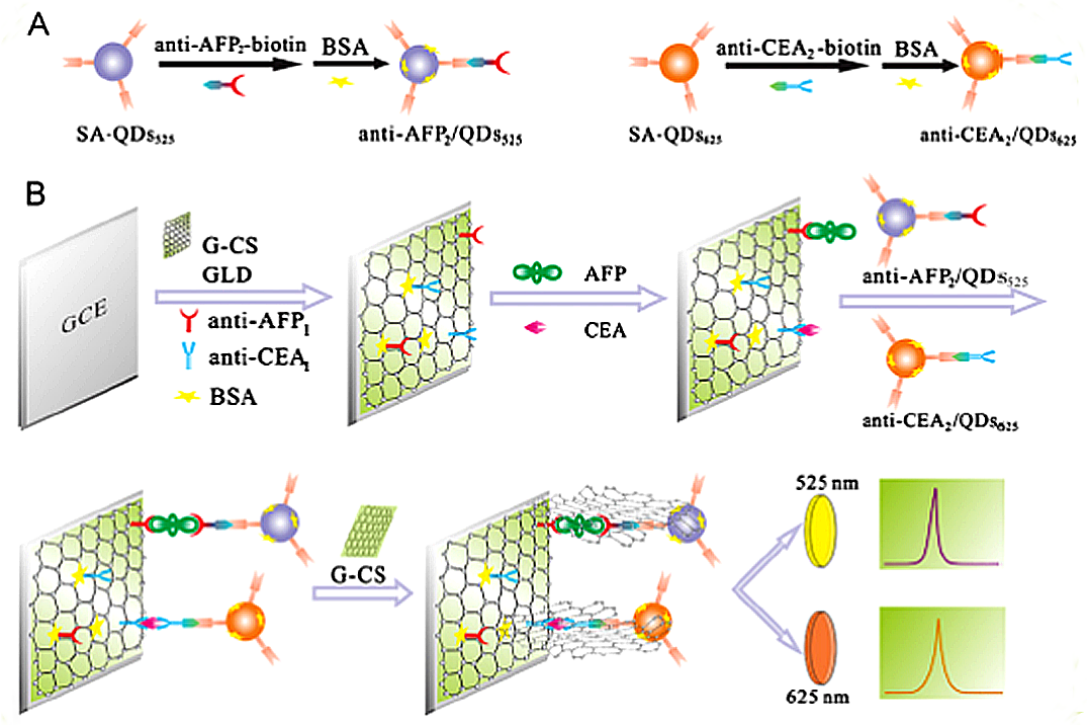

Figure 4. Schematic representation of (A) preparation of colloidal anti-AFP_2/QDs_{525} and anti-CEA_2/QDs_{625} conjugates; (B) procedure for the fabrication of immunosensor. Reprinted from Ref. [43] with permission of Elsevier Ltd.

A similar approach, but using core-shell Fe_3O_4- magnetic Au nanoparticles, was used to detect carbohydrate antigen (a cancer marker associated to ovarian cancer) at a concentration of 1.2 mU/mL as demonstrated by Liu *et al.*[44] Similar, but complementary strategies were utilised by Zhou *et al.* [45] with the development of a sandwich-type ECL immunosensor for detection of AFP, down to 0.2 pg/mL, using a combination of magnetic Fe_3O_4 nanoparticles with CdS QDs and Au NPs. Another interesting example of combination of nanomaterials is represented by the work of Li *et al.* [46]. In their work, 3D graphene was deposited on glassy carbon electrodes, followed by incorporation into the 3D graphene structure of CdSeTe QDs labelled with $Ru(bpy)_3^{2+}$-doped Si NPs. The as-proposed ECL sensor allowed detection of ultra-trace concentration of folic acid up to 3.5 aM with a 2-3 order of magnitude

improvement in the limits of detection compared to chromatographic, and other (non-ECL based) electrochemical methods. Similar procedures, using CdTe QDs, were adopted by Wang *et al.* to detect ochratoxin A down to 3 fg/mL in real samples[47] and by Zhang *et al.* to detect prostate specific antigen (PSA) with detection limits of *ca.* 3 pg/mL[48].

DNA detection is a rapidly expanding area in chemical analysis and achieving low detection limits is of paramount importance. ECL-based detection is an exciting strategy in order to achieve low detection limits, highly selectivity and repeatability. Recently, Zhang and coworkers developed a novel ratiometric approach for DNA biosensing[49]. The ratiometric approach is based on the use of dual excitation or dual emission dyes and can be applied to chemical species having at least two peaks in their excitation and/or emission spectrum. This method is extremely useful when the ratio of the fluorescence intensities at these wavelengths correlates with the concentration of the analyte, since it can reduce the influence from environmental changes such as scattering, path length, photobleaching etc. CdS QDs were coated on glassy carbon electeodes and ECL was performed in the presence of luminol as chromophore and H_2O_2 as coreactant. The ECL signal from CdS QDs can be effectively quenched by contacting them with Pt NPs through a biological binding event (in this specific case using mp53 oncogene, as a model DNA molecule), meanwhile the ECL from luminol can be enhanced by the presence of Pt NPs. Thus, the quenching of ECL from CdS QDs and the enhancement of ECL from luminol could indicate the same biological binding event. A molecular beacon (MB) containing a 20-base loop, which is complementary with the mp53 oncogene, was immobilized on CdS QDs followed the procedure highlighted in Figure 5. Pt NPs were then attached on CdS QDs surface by DNA hybridization between the MB and mp53 oncogene labelled on Pt NPs. By measuring the ratio of ECL intensities at two excitation potentials, this approach led to the detection of the concentration of target DNA in a wide range, from 5.0 fM to 1.0 pM. The proposed approach is generally applicable and adaptable to other biological binding events.

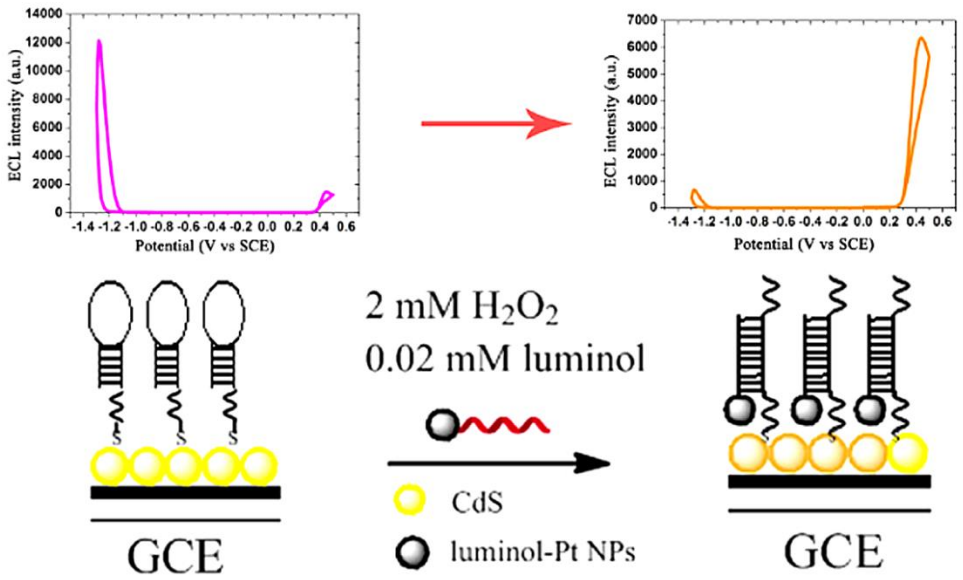

Figure. 5. Schematic of ECL ratiometric system. Reprinted from ref.[49] with permission of the American Chemical Society.

Recent advances on ECL detection with semiconducting quantum dots include the possibility of using spectral resolved ECL to detect single molecule events. This is achieved by lowering the background noise using charged-couple devices (CCDs)-monochromator and by proper functionalisation of QDs. In this respect, Zhang *et al.* reported the synthesis of dual-stabilisers CdSe QDs as a ECL label and CEA antigen as target molecule. This configuration allowed detection of CEA up to 0.1 fg/mL using only 20 µl of serum sample[50]. Furthermore, a similar approach was used by the same authors to detect AFP using ternary CdZsSe QDs[51] with limit of detection of 0.01 pg/mL and PSA up to 10 fg/mL using ternary CdZnSe QDs and dual-stabilisers CdZe QDs[52], respectively.

The versatility of ECL is represented not only by the combination of several classes of nanomaterials, but also by the possibility of integration with other analytical methods. A very exciting combination which is now receiving particular attention has led to the development of a novel analytical technique called electrochemiluminescence-energy transfer (ECL-ET)[53]. Luminescence resonance energy transfer (LRET) is an analytical technique for the detection of traces of biomolecules through non-radiative processes. In LRET a luminescent donor species transfers energy to a near acceptor species (luminescent or non-luminescent) via non-radiative dipole-dipole interactions[54]. The rate of energy transfer is highly dependent on the extent of spectral overlap and the distance between the donor and acceptor species. According to the different types of luminescence from the donor species, three major types of LRET have been defined, (i) fluorescence (or Förster) resonance energy transfer

(FRET)[55], [56], chemiluminescence resonance energy transfer (CRET)[57], [58], [59], and bioluminescence resonance energy transfer (BRET)[60], [61]. To achieve enhanced ECL-ET efficiency, optimum energy overlapping of donor/acceptor species is of crucial importance. In this respect, materials with tunable spectroscopic properties are particularly appealing as potential donor and acceptor species. Notably, the tunable emission wavelength and broad absorption spectra of QDs render them an ideal class of material for ECL-ET. QDs with near-infrared (NIR) emission (650–900 nm) are particularly attractive, as biological auto-fluorescence and tissue absorption are both at their minima in this wavelength range. So far many kinds of NIR-emitting QDs have been reported, such as CdSeTe, InAs, PbSe, CdP and CuInS, etc,[62], [63] and among them CdSeTe QDs have been of tremendous interest since their first report in 2003[64]. In comparison with other NIR-emitting QDs, CdSeTe QDs exhibit a very strong non-linear effect between composition and the absorption/emission energies, conferring them special optical and electronic properties not available from parent species such as CdSe and CdTe QDs. Therefore, the emission wavelength of CdTeSe QDs can readily reach NIR region by tuning the Te/Se molar ratio. This is a great advantage considering that CdSe QDs typically cover the region 480–620 nm in emission, while CdTe QDs (specifically 7 nm in size) can reach not more than 720 nm in emission[65]. However, the toxicity of Cd^{2+} released from CdSe or CdTe QDs represents a limitation for bioanalytical applications[66], [67], [68]. To overcome this issue, a solution is represented by using core-shell QDs, e.g. coating the Cd core with a suitable shell such as ZnS, even though two stringent conditions must be fulfilled: (i) the shell material should possess a much wider band gap than the core to suppress the exciton leakage into the shell; (ii) the core and shell materials should have similar lattice parameters so that the shell-growth occurs in an epitaxial manner, without the formation of structural defects which would hamper the quantum yield[69]. Typically, CdSeTe QDs are passivated with non-toxic ZnS shell to obtain core-shell CdSeTe/ZnS. However, for both CdSe and CdTe, the large lattice mismatches (>10%) relative to ZnS hinder the formation of high-quality core-shell QDs. This implies the development of novel synthetic procedure in aqueous media to fabricate NIR-emitting core-shell CdTeSe QDs with the desired optical properties and low biotoxicity. Examples of core-shell QDs are represented in Figure 6.

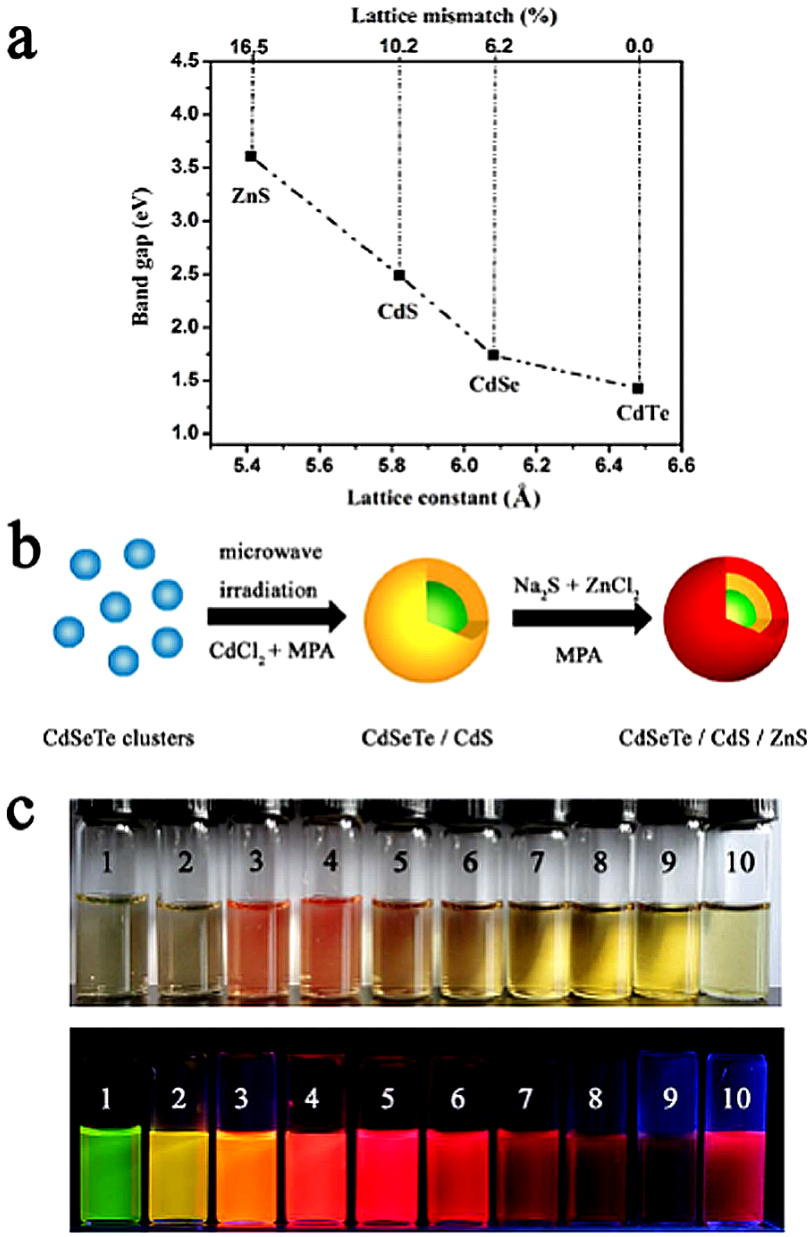

Figure 6. (a) Interrelationship between band gap energy, lattice constant, and lattice mismatch of bulk cubic CdTe, CdSe, CdS, and ZnS. (b) Synthetic procedures for the preparation of CdSeTe/CdS/ZnS QDs. (c) Photo images of the prepared CdSeTe/CdS QDs (samples 1–9) and CdSeTe/CdS/ZnS QDs (sample 10, relative to sample 7) taken under visible (upper) and UV light (lower), respectively. Reprinted from ref. [53] with permission of the Nature Publishing Group.

ECL-ET are widely utilised in medical diagnostics to develop novel sensing tools. A near-infrared (NIR)-ECL-ET aptasensor for detection of thrombin was developed by Wang *et al.*[70]. In this work core-shell CdTe/CdS QDs and Au nanorods were utilised for ECL-ET detection of thrombin in the presence of $S_2O_8^{2-}$ as coreactant. With QDs acting as donor and

Au nanorods as acceptor species, respectively, in the absence of thrombin the ECL signal was effectively quenched as a direct effect of ECL-ET between QDs and Au nanorods. In contrast, in the presence of thrombin, the NIR-ECL-ET become "turned-on" due to the effective replacement of Au nanorods with thrombin ascribed to the specific aptamer-protein affinity interaction. This allowed a remarkable increment of the ECL signal and the possibility to detect thrombin in serum in the concentration range 100 aM-10 fM with a detection limit of 3 fM. Later on, using CdSe/ZnS QDs and luminol but in the absence of co-reactant, Dong and coworkers were able to improve the detection limit of thrombin down to 1.4 fM[71]. A similar ECL-ET concept using CdS but with Au NPs was used for studies of DNA binding with proteins [72]. Another interesting approach that led to a significant enhancement in the ECL-ET signal involved the formation of CdS:Eu nanocrystals. In this work Zhou *et al.* were able to detect target DNA in the range 10 aM-10 pM in the presence of $S_2O_8^{2-}$ as co-reactant[73]. In this case, the addition of Eu^{3+} ions has a beneficial effect by creating new surface states that enhance the ECL signal. Interestingly, the ECL signal has two spectral bands, the first one at 450-550 nm from CdS and the second one at 600-700 nm caused by the energy transfer between CdS and Eu^{3+} ions. Further recent and significant development in ECL-ET is the combination of CdS:Eu nanocrystals with biocompatible $Ru(bpy)_3^{2+}$-doped silica nanoparticles (RuSi) for detection of prostate specific antigen (PSA)[74]. This combination enhanced the ECL-ET signal up to *ca.* 5-fold due to efficient ECL-ET and high $Ru(bpy)_3^{2+}$ quantum yield leading to reaching detection limit for PSA up to 1 fg/mL[74]. In a similar procedure Wu *et al.* utilised graphene oxide- Au NPs previously functionalised with RuSi NPs and chitosan as the donor composite, with Au/Ag_2S NPs as the acceptor[75]. This work led to ECL-ET detection of target DNA in the range from 10 aM-10 pM in the presence of TPrA as co-reactant. The versatility of ECL is clearly evident when is combined with other analytical techniques. One of the most significant combination is represented by the surface-enhanced electrochemiluminescence (SEECL)[76], despite the first seminal work on surface plasmon coupled with ECL was reported by Lakowicz in 2004[77]. In this work, it has been shown that electrochemically-generated excited states of $Ru(bpy)_3^{2+}$ can excite the surface plasmon of Au thin films. This concept demonstrated that surface plasmon can be excited by excited states of luminophores. Since then, studies of the interaction between the ECL of semiconductor QDs and the localised surface plasmon resonance of noble metal nanostructures has been investigated[78], [79]. The mechanism of ECL, summarised in Figure 7 occurs in two steps.

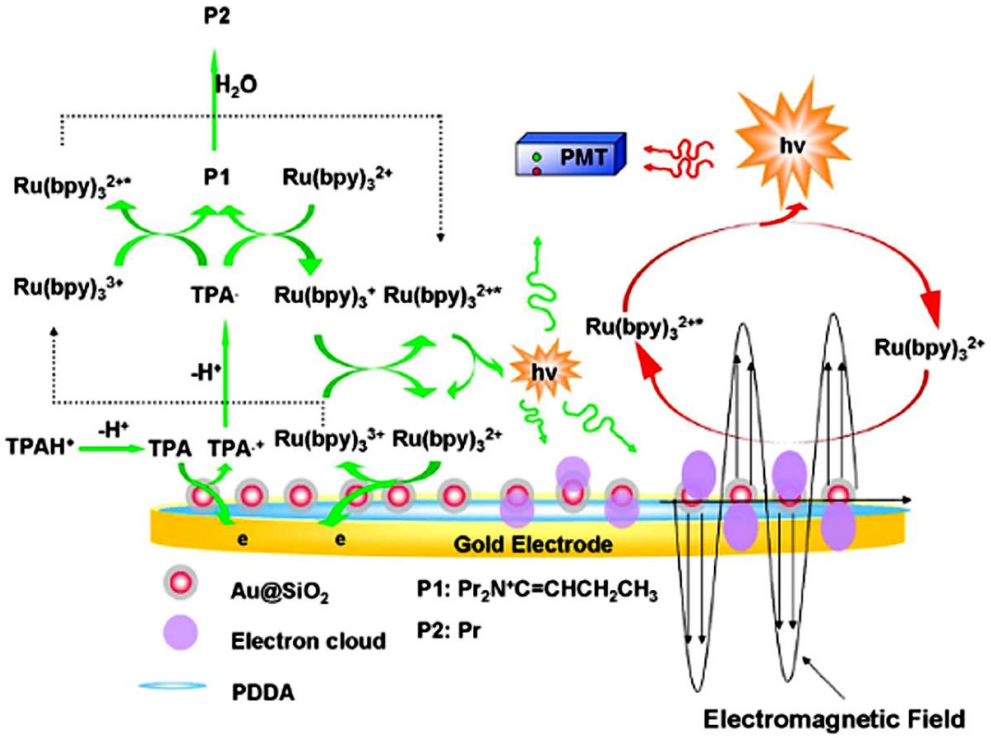

Figure 7. Schematic diagram of SEECL. Reprinted from Ref. [76] with permission of the Nature Publishing Group.

The first step is the electrochemical generation of excited states of the luminophore, $Ru(bpy)_3^{2+*}$ with TPrA, the second step involves the generation of the plasmon resonance at the surface of Au NPs in a similar way as previously demonstrated by Lakowicz in the case of a thin Au film [77]. The enhancement in the ECL signal can be explained with similarity with fluorescence. In this case the ECL efficiency can be quantified by the gain in the relative molecular detection efficiency, MDE. At the position r_0, MDE can be expressed by the expression:

$$MDE(r_0) = \Gamma_{exc}(r_0)\ x\ Q\ x\ MCE(r_0) \qquad (33)$$

Where $\Gamma_{exc}(r_0)$ is the excitation rate, Q is the ECL quantum yield, and $MCE(r_0)$ represents the molecular collection efficiency function at point r_0.[76]. This mechanism is proposed on the ground that the luminophore is excited by a propagating or an evanescent electromagnetic field. Because the localised surface plasmon resonance induced magnetic field belongs to electromagnetic field, then it is reasonable to assume that the electromagnetic field can excite the luminophore from the ground to the excited state leading to an increase of the excitation rate $\Gamma_{exc}(r_0)$. Also, the electromagnetic field increases the emission factor ($Q\ x\ MCE(r_0)$) of $Ru(bpy)_3^{2+*}$. Key for the ECL enhancement is the control of the inter-distance between

luminophore and Au NPs. Then, the same authors demonstrated the suitability of SEECL for detection of CEA in human serum[80]. As one of the most important cancer biomarker, CEA detection has received significant attention. $Ru(bpy)_3^{2+}$-doped SiO_2 NPs were used as ECL luminophores with AuNPs utilised as LSPR source to enhance the ECL signal. Two different kinds of aptamers specific to CEA were modified on the surface of SiO_2 NPs and Au NPs. This configuration and TPrA as co-reactant allowed the detection of CEA with detection limits of *ca.* 1.5 ng/mL in human serum and demonstrated the suitability of the surface plasmon resonance to amplify the ECL signal (see Figure 8).

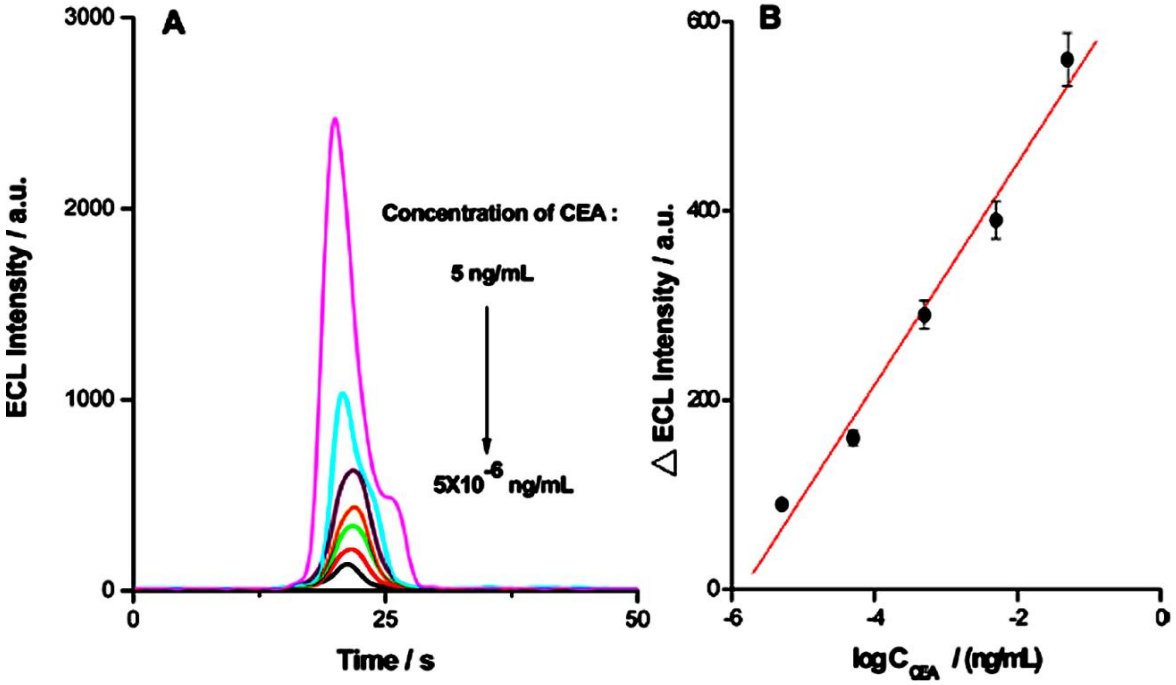

Figure 8. (A) Concentration-dependent ECL of the biosensor ad different CEA concentrations (from 5 (top), to 5× 10−6 ng/mL (bottom), respectively. (B) The calibration curve for quantification of CEA. Experimental conditions: 0.1M pH 7.4 PBS and 1 mM TPrA. The scan rate is 100 mV/s for all measurements. Reprinted from ref. [80] with permission of the American Chemical Society.

Previously, the same authors utilised a slightly modified experimental set-up to detect ultra-trace concentrations of Hg^{2+}[81]. Specifically, Au nanorods and T-rich DNA were self-assembled on the surface of gold electrode. In the presence of Hg^{2+}, the conformation of ss-DNA probes changed towards a hairpin-like structure with formation of a T-Hg^{2+}-T structure (see Figure 9). The insertion of a luminophore such as $Ru(bpy)_3^{2+}$ into the grooves of the hairpin structured DNA probes generated ECL emission, further enhanced by the localised surface plasmon resonance of Au nanorods. The ECL intensity of the sensor increased linearly with the concentration of Hg^{2+}, with a detection limit of 10 fM.

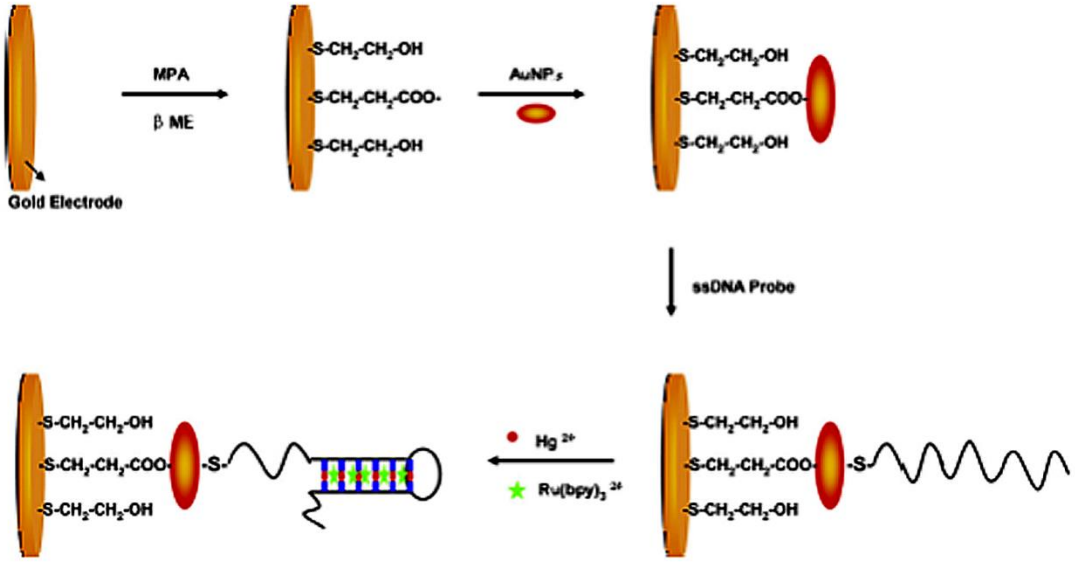

Figure 9. schematic of SEECL detection of Hg^{2+}. Reprinted from Ref. [81] with permission of Elsevier Ltd.

Later on, the same concept has been utilised by the same authors to detect PSA in whole blood without sample treatment achieving detection limits for PSA of 2 pg/mL[82].

ECL with arrays of nanowire, nanotube and nanodisk electrodes

ECL at the nanoscale presents attractive features[74], however, particularly for the case of working with electrodes of nanometric dimensions, it represents also a great challenge, particularly from the technical view point. One important advantage to use smaller and smaller electrodes lies in the fact that one could perform almost punctual ECL measurements in extremely localized sites, such as biological sub-cellular organelles, discontinuity points in heterogeneous or microporous surfaces, as well as in micro- and nanostructured sensors and biosensors. Pushing the dimensional limit of ECL in the hundreds of nanometer range or lower presents fascinating prospects also from improving fundamental knowledge on ECL mechanism. For instance, it is not known what could be the effect of decreasing the dimension of the ECL reaction layer when making it dimensionally comparable with the thickness of the electrochemical double layer (that is in the few tens of nanometer dimension). The main technical problem to achieve these goals lies in the fact that the intensity of ECL emission at an individual electrode of nanometric dimension can be too feeble to be detected. For instance, Jiang and coworkers observed that ECL emission from a

recessed nanoring electrode (180 nm thick, 30 µm ring diameter, 30 µm recession depth) cannot be detected by usual ECL measurement methods[83]. Note that ECL at a ITO microdisk electrode of the same diameter (namely, 30 µm) was easily detected. In principle, these problems could be overcome by using innovative ECL detection approaches, but at the present state of the art, detection of weak ECL emission signals, localized at the nanoscale, is still an open challenge. A way to circumvent the problem is to use arrays of nanoelectrodes, instead of individual ones, so taking advantage of relevant amplification effects on the overall intensity of ECL emission, that are operative when overlapping conditions between the reaction layers at neighboring electrodes occur.

Both from a microfabrication and ECL detection viewpoint, one can distinguish two types of arrays of nanoelectrodes exploited for ECL generation: i) arrays of conductive nanowires or nanotubes, assembled in nano-arrangements; ii) arrays of nanoelectrodes produced in geometrically controlled nanostructures.

The first group includes macro- and microelectrodes modified by deposition of conductive nanomaterials, typically carbon nanotubes (CNTs), deposited by casting, sprying, printing or similar approaches.

For ECL applications, CNTs are attractive since they are characterized by a fast electrochemical kinetics for the oxidation of tertiary amines (typical co-reactants in ECL) while water oxidation (an undesired side reaction in ECL) presents a high overpotential on this class of nanomaterials[84]. CNTs have been deposited on different supporting electrode materials, such as Au, ITO or glassy carbon (GC). For instance, Rusling and coworkers obtained CNTs arrays arranged in vertically aligned structures named carbon nanotubes forests, which were applied at first for electrochemical detection[85], [84], to be further developed to prepare an ECL immunosensor for immunoglobulin G (IgG)[86]. In this sensor, capture anti-IgG antibodies were bound onto vertically aligned single wall carbon nanotubes (SWCNTs) via amide bond formation with the carboxylic groups present on the CNTs wall. ECL was generated by binding both a suitable $Ru(bpy)_3^{2+}$ derivative and IgG on amine functionalized silica nanoparticles. The sensor was able to detect IgG down to the pico-molar level.

This ECL approach was further implemented to develop an ECL immunoarray incorporated into a prototype microfluidic device, schematized in Figure 10[87]. It was demonstrated that the device is suitable for highly sensitive protein detection and can be used for the accurate and sensitive determination of PSA and interleukin-6 (IL-6) in serum.

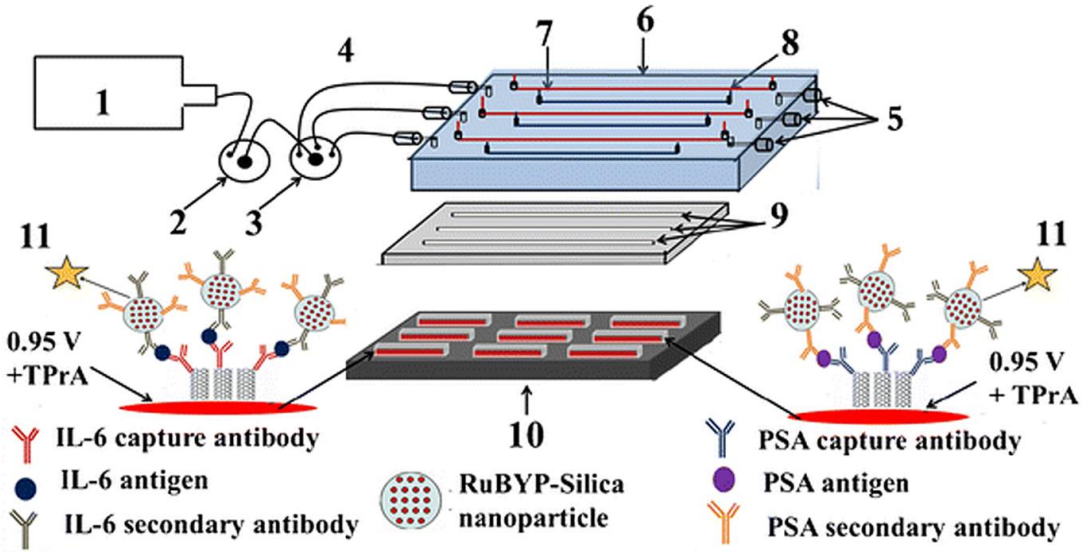

Figure 10. Design of microfluidic ECL array: (*1*) syringe pump, (*2*) injector valve, (*3*) switch valve to guide the sample to the desired channel, (*4*) tubing for inlet, (*5*) outlet, (*6*) poly(methylmethacrylate) (PMMA) plate, (*7*) Pt counter wire, (*8*) Ag/AgCl reference wire (wires are on the underside of PMMA plate), (*9*) polydimethylsiloxane (PDMS) channels, (*10*) pyrolytic graphite chip (PG) (2.5 × 2.5 cm) (*black*), with hydrophobic polymer (*grey*) to make microwells. Bottoms of microwells (*red rectangles*) contain primary antibody-decorated SWCNT forests, (*11*) ECL label containing RuBPY-silica nanoparticles with cognate secondary antibodies is injected to bind to the capture protein analytes previously bound to cognate primary antibodies. ECL is detected with a CCD camera. Reprinted from Ref.[87] with permission of Springer.

The following evolution of this concept is represented by an automated multiplexed ECL immunosensor[88] suitable for the simultaneous detection of four cancer biomarkers, namely PSA, prostate specific membrane antigen (PSMA), platelet factor-4 (PF-4) and IL-6.The device can detect the four analytes in 36 min, with detection limits in the 10-100 fg/mL range. Note that ECL was generated at 0.95 V, using TPrA oxidation to stimulate ECL emission, according to the so called revisited route for ECL emission, proposed by Miao, Choi and Bard[89] . A CCD camera was used to measure the luminescence emitted from the array.

A sensitive ECL immunosensor for marine toxins was developed by Zamolo *et al.* [90], by exploiting MWCNTs difunctionalized by the procedure summarized in Figure 11.

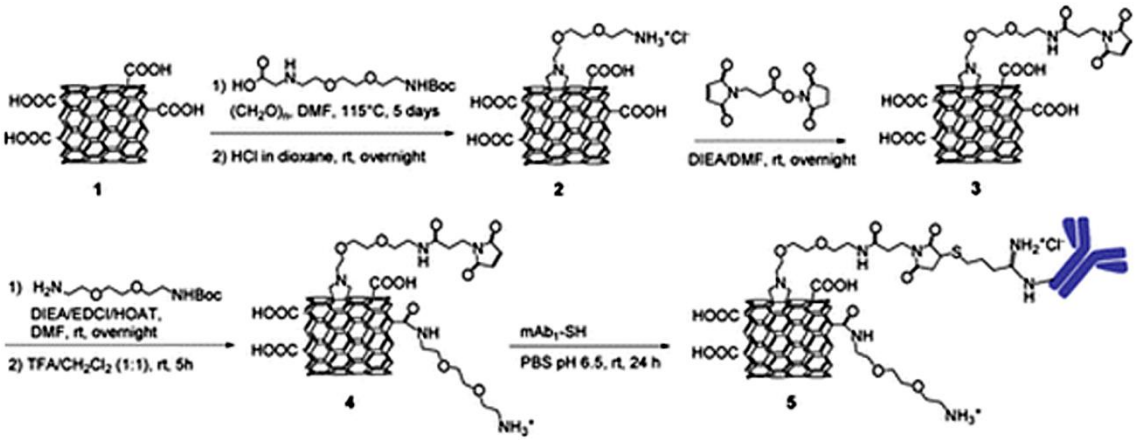

Figure 11. Preparation of Doubly Functionalized MWCNT. Reprinted from Ref.[90] with permission of the American Chemical Society.

The so introduced maleimido groups are exploited to bind onto the CNT the capture antibody, while the amino terminated functionalities are exploited to graft the functionalized nanotube on a ITO electrode coated with electropolymerized N-succinimidyl polyacrylate (see Figure 12). Finally, the capture Ab binds the analyte, namely palytoxin (PITX) and the recognition event is detected using a sec-Ab labeled with a $Ru(bpy)_3^{2+}$ derivative. By using the ECL sensor, PITX was successfully detected in real samples (mussels), with a quantification limit of 2.2 µg/kg that is significantly lower value than the one achieved via LC-MS/MS.

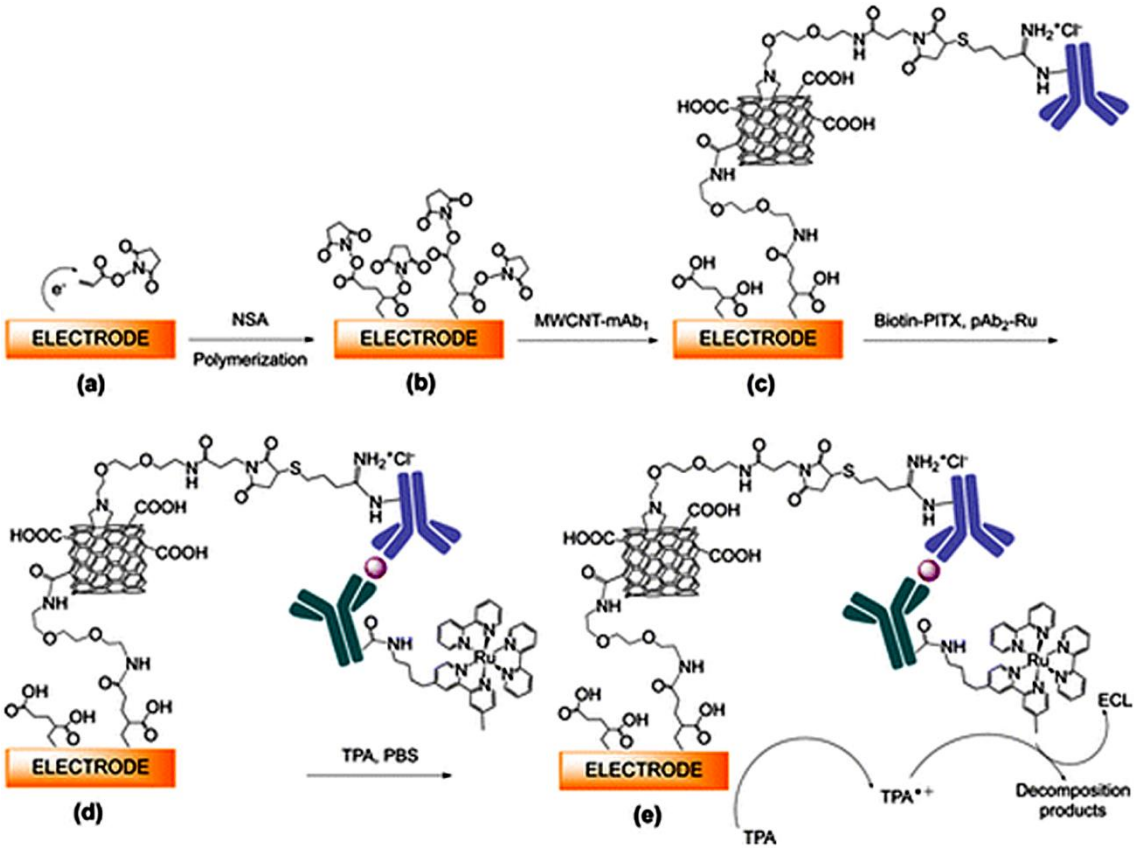

Figure 12. (a) Electrografting of ITO with NSA. (b) Functionalization of MWCNT–mAb_1. (c) Addition of biotin–PlTX (purple sphere) followed by pAb_2-Ru. (d) Addition of the TPRA co-reactant. (e) ECL development. Reprinted from Ref.[90] with permission of the American Chemical Society.

Valenti et al. [91] studied an original procedure to produce transparent electrodes for ECL use, where CNTs constitute the electrode conductive layer, without the need of using any other electrode material. The transparent CNT electrode was fabricated by careful evaporation onto a transparent substrate (either glass or polyethylene terephthalate) of a CNT solution in tetrahydrofuran, after suitable chemical reduction-reoxidation steps performed under controlled atmosphere. The CNT-transparent electrode demonstrated electrocatalytic properties superior to classical ITO transparent electrodes, as evaluated from the cyclic voltammetric peak-to-peak potential separation values, which, for reversible redox probes, matches the 60 mV theoretical value, even at high scan rates. The ECL emission efficiency, for the $Ru(bpy)_3^{2+}$/TPrA systems, was ten times higher than with ITO electrodes. As a proof of concept, ECL imaging from $Ru(bpy)_3^{2+}$ functionalized silica microbeads was proved as a model to mimic single cell visualization.

Nanotubes other than CNTs have been also used for improving ECL emission. Dai and coworkers developed a sensitive and stable ECL platform made of titanate nanotubes (TNTs)

incorporated in a Nafion layer[92]. The photocatalytic activity of the TNTs was exploited to enhance luminol ECL emission using H_2O_2 as the coreactant or analyte. In principle, the platform can be combined with suitable oxidase enzymes which use oxygen as electron acceptor to produce H_2O_2, catalyzing the oxidation of various biochemical substrates. However, the authors did not present any applicative example to confirm experimentally this prospect.

Numerous studies developed in the last years have demonstrated that the efficiency of diffusion at electrode/solution interfaces increases dramatically when the critical dimensions of the electrode are lowered down to the nanometer range[93], [94], [95] .

Because of possible co-operation between neighbouring electrodes, these effects are even more relevant, and can be more easily detected, when using arrays of nanoelectrodes, for reviews see e.g. [96], [97]. In nanoelectrode ensemble (NEE) and in nanoelectrode array (NEA), individual nanoelectrodes are randomly or orderly distributed, respectively.

NEAs fabrication requires the use of bottom-up nanotech approaches, such as electron or ion-beam lithography or nanoimprinting[98], [99]. NEEs are typically fabricated by bottom-up approaches, the most widely used being electrochemical or electroless deposition of a metal in the pores of microporous templating membranes, introduced by C.R. Martin and coworkers[100], [101]. NEEs/NEAs are characterized by improved electrochemical performances because their nanoscopic dimensions reflect in very low capacitive currents, so dramatically lowering detection limits[101], [102], [103], [104], [105] . Moreover, arrays have the advantage to furnish significantly higher currents than individual nanoelectrodes, without requiring sophisticated electronic amplification of current, nor shielding with a Faraday cage.

The enhanced efficiency of mass transport at nanoelectrodes has dramatic consequences on the role played by the kinetics of the electron transfer[100], [106], [107], [108] or of chemical reactions associated with the electron transfer, including those reactions involved in ECL emission. Indeed, the increased efficiency of diffusion at nanoelectrodes means that other kinetic steps (e.g. heterogeneous electron transfer or chemical reactions) can become the bottleneck of the overall electron transfer process. Up to now, the electrochemical behaviour of redox processes at NEEs/NEAs have been studied mainly for the case of rather simple electron transfer processes, involving the direct reduction/oxidation of reversible or quasi-reversible redox probes, eventually coupled with very fast (and therefore kinetically un-influent) chemical reactions[109], [110], [111]. This holds for theoretical studies as well[112], [113].

As far as ECL generation at arrays of micro- or nanoelectrodes is concerned, only few papers dealt with ECL generation at microband electrodes and microfabricated interdigitated

electrode arrays[114], [115], [116]. Recently, bipolar electrochemistry was used to stimulate ECL emission from arrays of microband electrodes or dispersions of conductive micro-objects [117], [118].

A bipolar electrode (BPE) is an electronic conductor at the two ends of which two opposite electrochemical processes (namely, an oxidation on one side and a reduction on the other side) occur, without the need of a direct contact with an external power source; for recent reviews see e.g.[119], [120], [121]. In addition to BPE(s), the functioning of a bipolar electrochemical cell requires two auxiliary electrodes, named driving electrodes, which are connected to an external power source to induce the polarization of the BPE(s). Bipolar electrochemical cells can be designed as open bipolar electrochemical cells (OBPECs) and closed bipolar electrochemical cells (CBPECs).

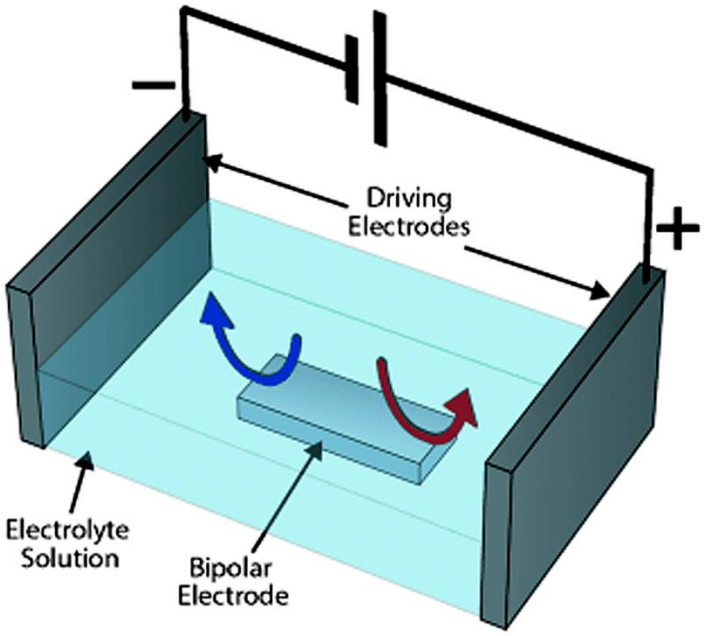

Figure 13. Graphic representation of an open bipolar electrochemical cell. Reprinted from Ref.[119] with permission of Wiley-VCH.

As shown in Figure 13, in OBPEC, the BPE is a conductor dipped in an electrolyte; the application of a suitable potential difference between the driving electrodes generates a current which flows via ionic or electronic pathways. The electronic path is maximized when using a conductive BPE in a resistive solution. If a voltage is applied between the driving electrodes, a potential difference (ΔV) is generated between the two poles of the BPE and the electrolyte solution is produced because of the polarization of the latter, according to eq.34:

$$\Delta V = E \cdot l \qquad (34)$$

where E is the intensity of the electric field and l is the length of the BPE.

Therefore, in order to apply bipolar electrochemistry in open configuration to nanosized substrates, electric fields in the order of tens of kV/m must be used[122] .

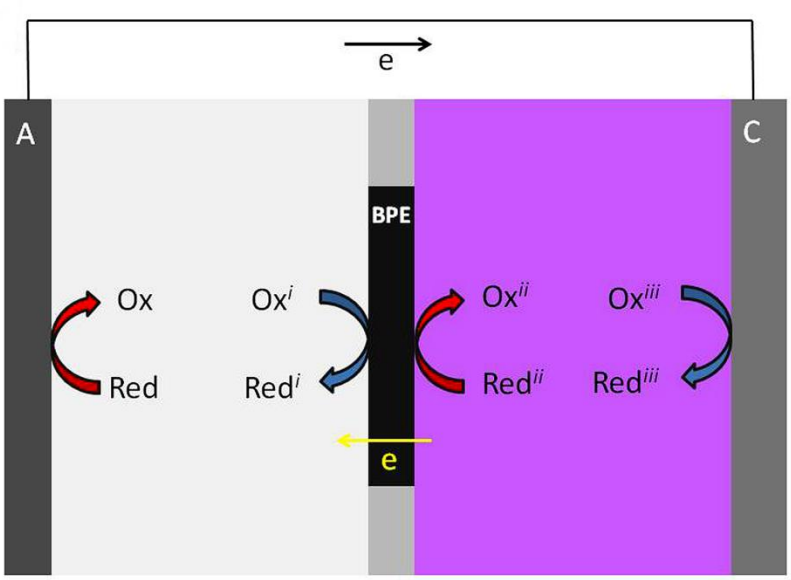

Figure 14. Graphic representation of closed bipolar electrochemical cell; A and C are the driving electrodes used as anode and cathode, respectively. Reprinted from Ref.[123] with permission of Wiley-VCH.

This limit can be overcome by using CBPEC, where a conductive substrate (the BPE) obstructs the cell dividing it into two half-cells each containing a driving electrode (Figure 14). If the half-cells contain suitable concentrations of electroactive electrolytes, ΔV at the BPE does not depend on its dimension, being substantially equal to the potential difference between the driving electrodes. Note that in this configuration, all the current flows only through the BPE substrate. In CBPECs, the BPE can be an individual conductive object or a composite material in which conductive particles are embedded in an insulating matrix. It was recently demonstrated that using a CBPEC it is possible to perform bipolar electrochemistry even at ensembles of nanowire electrodes of 30-60 nm diameter and few µm length, by using low intensity electric fields, in concentrated electrolyte solutions [123]. Since the cell is composed of two separated compartments, the two different electrolyte solution can operate in distinct experimental conditions such as temperature, or, viscosity.

Using the CBPEC approach, Wang and coworkers, developed a multichannel closed bipolar array suitable for ECL sensing[124]. It is based on a microporous poly(ethylene terephthalate) (PET) membrane where the pores have been filled with gold nanowires (420 nm diameter) deposited electrochemically or chemically. The detection principle is schematized in Figure 15. The ECL readout was detected at the compartment on the left, being coupled with a reduction process occurring in the compartment on the right. By this design, it was possible to detect a variety of targets which including oxidants, coreactants, quenchers, and biomarkers by using the same $Ru(bpy)_3^{2+}$/TPrA ECL readout.

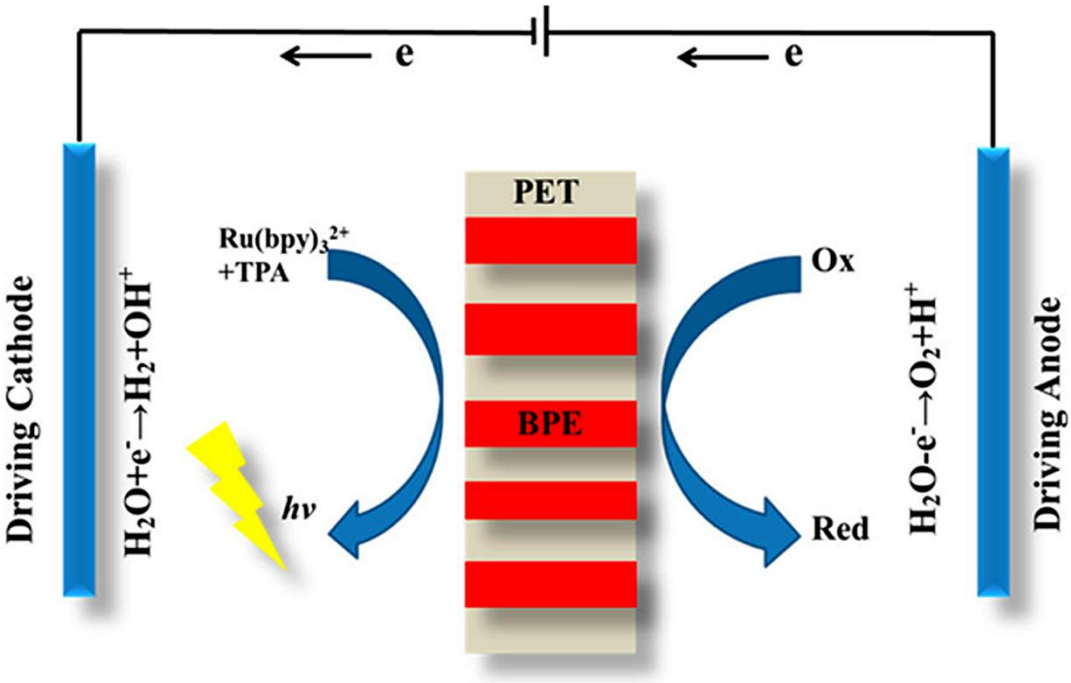

Figure 15. Fundamental principle of the multichannel closed bipolar electrode ECL sensor for analyte detection. Note that the figure is not to scale and the BPEs are indeed gold nanowires with 210 nm. radius. Reprinted from Ref.[124]with permission of the American Chemical Society.

The multichannel PET membrane, after exposure to ion-beam and UV sensitization, can be etched to the desired pore diameter by NaOH. Using ECL at the CBPEC array several analytes were detected such as dopamine, H_2O_2, AFP, and carcino- CEA. The practical applicability was tested by analyzing AFP and CEA in human serum, confirming the potentiality of the device for multi-analysis purposes.

A novel ECL immunosensor for celiac disease diagnosis, based on NEEs was recently proposed [125]. The sensing strategy was based on the spatial segregation between the sites where the initial electrochemical reaction and ECL emission occur. As shown in Figure 16, tissue transglutaminase (tTG) was used as capture agent. It was immobilized on the

polycarbonate (PC) surface of the track-etched membrane used as template to fabricate the NEE, and exploited to bind the target tissue transglutaminase antibody (anti-tTG). This was reacted with a sec-Ab labeled with a ruthenium luminophore. Other details of the detection strategy are illustrated in the caption of Figure 16.

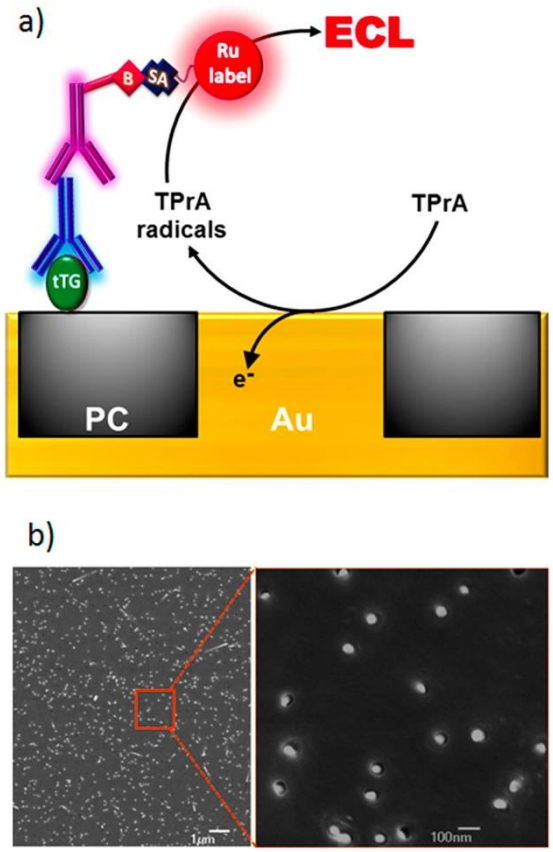

Figure 16. a) Scheme showing the design of the immunosensor (not in scale). The PC surface is first modified with the capture protein, tTG. The assay is performed by incubating it with a sample containing the target (i.e. anti-tTG antibody) and then in a solution of a biotinylated secondary antibody. The final step consists in attaching the ECL label by exposing the immunosensor to a solution containing a streptavidin-modified $Ru(bpy)_3^{2+}$ complex (SA-Ru). Oxidation of TPrA occurs at each Au nanoelectrode of the NEEs and the resulting radicals, $TPrA^{\bullet+}$ and $TPrA^{\bullet}$, diffuse over short distances and react with the luminophore label attached to the PC to generate the ECL emission. Note that the figure is not to scale and the Au nanoelectrodes have a nominal diameter of 30 nm. b) Field emission scanning electron microscopy (FE-SEM) images of a gold-NEE at two magnifications. Reprinted from Ref.[125] with permission of the American Chemical Society.

It is worth stressing that the electroactive surface is composed by an ensemble of gold nanodisk electrodes with radius of 15-25 nm (see Fig. 16 b) and the biorecognition component (including the ECL label) is immobilized on the polycarbonate template in which the nanoelectrodes are embedded..Voltammetric and ECL analyses demonstrated that, in this sensor, the ruthenium complex is not oxidized directly at the surface of the nanoelectrodes, but ECL is generated solely via TPrA oxidation at 0.88 V vs. Ag/AgCl to produce $TPrA^{\bullet+}$ and $TPrA^{\bullet}$ radicals, according to the scheme [82], [120]:

$$TPrA^{\bullet+} \leftrightarrows TPrA^{\bullet} + H^{+} \quad (35)$$

$$TPrA^{\bullet} + PC—\cdots—Ru(bpy)_3^{2+} \leftrightarrows Im^{+} + PC—\cdots—Ru(bpy)_3^{+} \quad (36)$$

$$TPrA^{\bullet+} + PC—\cdots—Ru(bpy)_3^{+} \leftrightarrows TPrA + PC—\cdots—Ru(bpy)_3^{2+*} \quad (37)$$

$$PC—\cdots—Ru(bpy)_3^{2+*} \rightarrow PC—\cdots—Ru(bpy)_3^{2+} + h\nu_{ECL} \quad (38)$$

where Im^{+} is the iminium product and $PC—\cdots—Ru(bpy)_3^{2+}$ represents the ruthenium label attached to the PC surface *via* the biorecognition chain described in Figure 16.

Analysis performed in human serum samples, demonstrated that the NEE-based ECL immunosensor is able to discriminate between healthy individuals and celiac patients.

Insight into the parameters which influence the generation of ECL at arrays of nanoelectrodes, was recently obtained by preparing and studying NEAs with highly-controlled geometry [126]. The substrate electrode material used to this aim was boron-doped diamond (BDD). BDD is particularly attractive for ECL studies thanks to its high chemical and electrochemical stability, satisfactory electrical conductivity and wide potential window[126], [127] The preparation of arrays and ensembles of BDD nanoelectrodes have been previously achieved by nanoparticles templated procedure [123], by nanosphere lithography [124] and by e-beam lithography[128].

In this work, NEAs with 16 different geometries were fabricated on the same BDD substrate by using a highly controllable e-beam lithographic procedure [129] . A multiple nanoelectrode arrays platform (MNEAP) was prepared, being composed by arrays of individual electrodes with critical size from 100 to 1000 nm (see Figure 17).

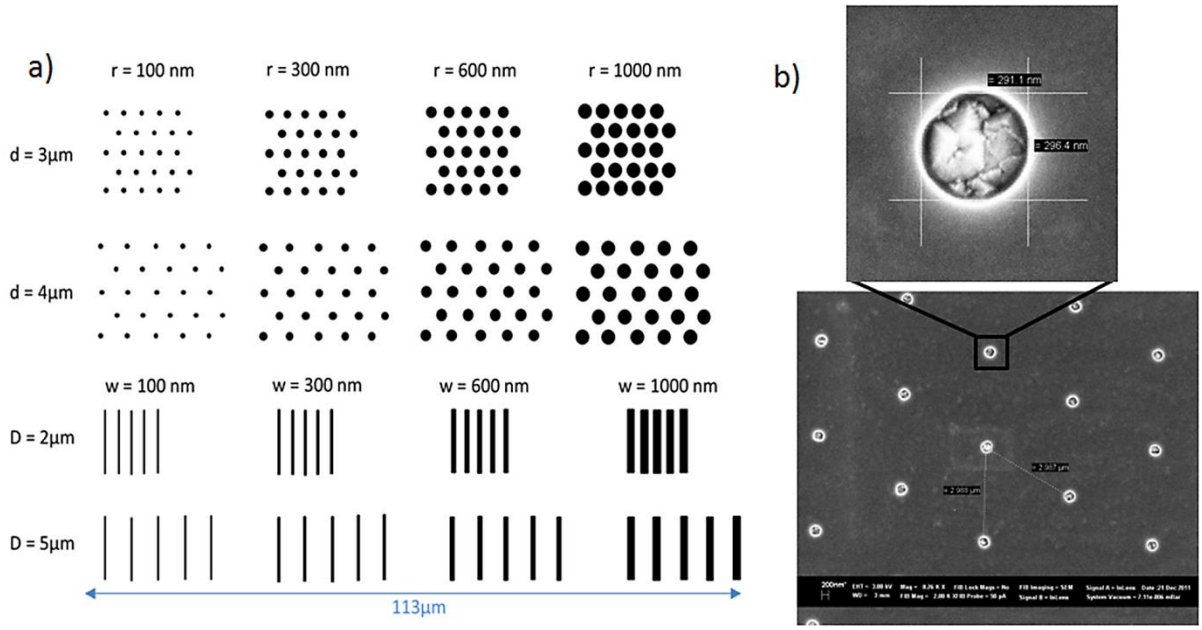

Figure 17. (**a**) Schematic drawing of the fabricated MNEAP. The parameters *r*, *d*, *w* and *D* correspond to the disc radius, the centre-to-centre distance between discs, the width of the bands and the pitch between the bands, respectively. The identification key of the NEAs in the platform is displayed in ESM Fig. S1. (**b**) Scanning electron micrographs of a BDD-based NEA constituted by nanodisc electrodes with $r = 150 \pm 10$ nm and $d = 3$ µm at different magnifications. Reprinted from Ref.[130] with permission of Springer.

By microscopic ECL imaging by a CCD camera, it was possible to capture simultaneously, in a single image, the ECL emitted from the different NEAs, allowing to study the intensity and spatial distribution of the ECL emission as a function of the geometrical features of the array as well as of the concentration of the TPrA coreactant (see Figure 18). The analysis of the ECL imaging data indicated that the ECL emitting zone scales inversely with the coreactant concentration as well as significantly more intense ECL signals were detected for NEAs operating under overlap conditions. Note that individual ECL emission at nanoelectrodes with critical dimension as small as 300 nm were imaged.

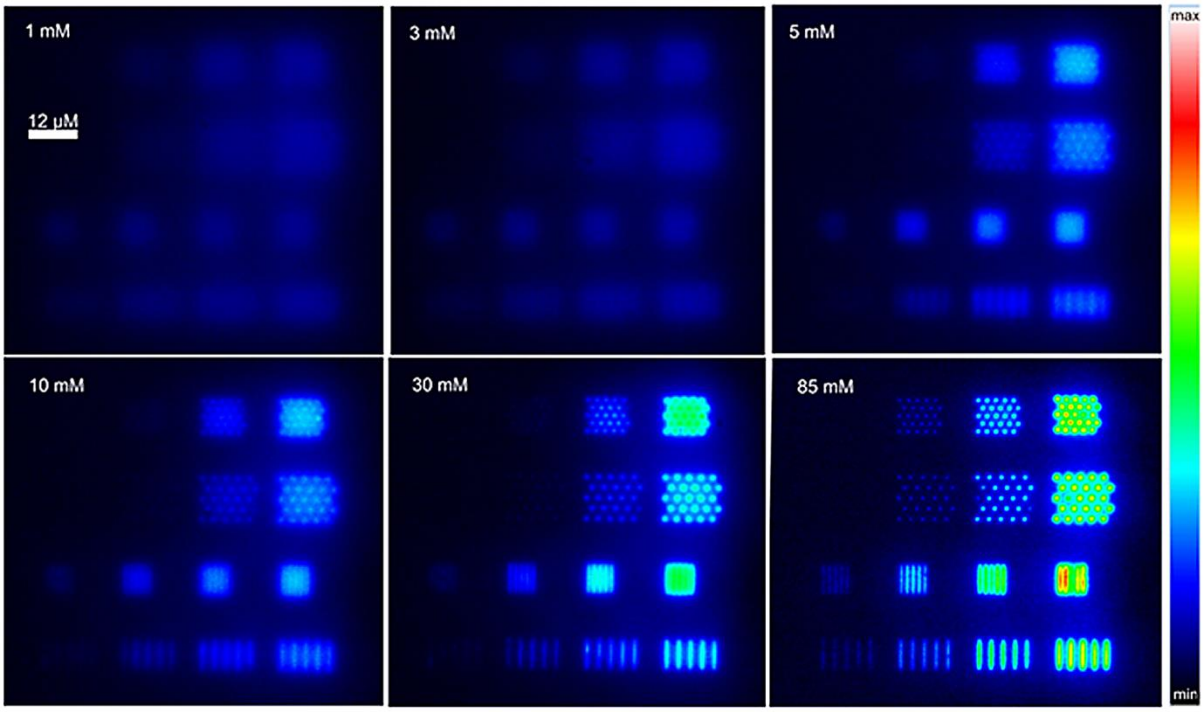

Figure 18. ECL images of a BDD-NEA obtained in phosphate buffer (pH 7.4) containing 1 mM $Ru(bpy)_3^{2+}$ and increasing concentrations of TPrA (indicated in top-left corner of each box). Images were recorded in the dark with a ×50 objective when applying a constant potential of 1.2 V vs. Ag/AgCl/KCl. All images were coded according to the same false colour scale (right). Reprinted from Ref.[130] with permission of Springer..

Conclusions

Analytical applications based on ECL have dramatically increased over the last five years and the impact they are having especially in bioanalyses and medical diagnostics is tremendous. Simplicity in instrumentation and high sensitivity make ECL a very appealing analytical technique characterised by fast response times, ease of use, and unprecedented sensitivity up to the atto molar level. All these achievements have been possible thanks to the synthesis of highly luminescent nanomaterials such as quantum dots, as well as by the improved detection capabilities offered by arrays of nanoelectrodes with very low background current, along with various strategies for bioconjugation of biomolecules on nanomaterials. Therefore, ECL is set to play a key role in the field of analytical sensors and bioanalysis, and recent applications can lead, in the near future, to develop novel portable and highly miniaturized and sensitive devices suitable for many applications, e.g. for biomedical use or the decentralized monitoring of chemical and biochemical hazards. These applications rely on highly selective and sensitive instrumentations, coupled with friendly use and affordable cost, all in miniaturized sensing devices, thank to the use of nanomaterials and nanoelectrodes

which warranty high ECL signals from sensors with very small geometric area. In this respect, ECL with nanodots and nanoelectrodes fulfils all these criteria and it is highly likely that future developments, especially in medical diagnostics, will grow dramatically.

From an experimental viewpoint, future research efforts should be directed in the direction of improving the spatial resolution and sensitivity necessary to face with the measurement and imaging challenges of ECL detection from nanometre sized objects. The recent experimental studies presented in this review indicate the lines of development to be followed. However they outline the requirement of being supported by theoretical studies capable to model ECL emission from arrays of nanometric ECL emitters operating under different experimental conditions, e.g. overlapping or non-overlapping configurations.

References

[1] M. M. Richter, *Chem. Rev.* **2004**, *104*, 3003-3036.
[2] K. A. Fahnrich, M. Pravda, G. G. Guilbault, *Talanta* **2001**, *54*, 531-559.
[3] W. J. Miao, *Chem. Rev.* **2008**, *108*, 2506-2553.
[4] R. J. Forster, P. Bertoncello, T. E. Keyes, in *Annu. Rev. Anal. Chem.* **2009**, *2*, 359-385.
[5] D. M. Hercules, *Science* **1964**, *145*, 808-809.
[6] K. S. V. Santhanam, A. J. Bard, *J. Am. Chem. Soc.* **1965**, *87*, 139-140.
[7] N. Harvey, *J. Phys. Chem.* **1928**, *33*, 1456-1459.
[8] Y. Zhang, Q. Wei, *J. Electroanal. Chem.* **2016**, *781*, 401-409.
[9] F. Lisdat, D. Schafer, A. Kapp, *Anal. Bioanal. Chem.* **2013**, *405*, 3739-3752.
[10] H. Zhou, J. Liu, S. S. Zhang, *TrAC, Trends Anal. Chem.* **2015**, *67*, 56-73.
[11] W. W. Zhao, J. Wang, Y. C. Zhu, J. J. Xu, H. Y. Chen, *Anal. Chem.* **2015**, *87*, 9520-9531.
[12] H. Jin, R. J. Gui, J. B. Yu, W. Lv, Z. H. Wang, *Biosens. Bioelectron.* **2017**, *91*, 523-537.
[13] R. B. Xie, Z. F. Wang, W. Zhou, Y. T. Liu, L. Z. Fan, Y. C. Li, X. H. Li, *Anal. Methods* **2016**, *8*, 4001-4016.
[14] Y. Q. Dong, J. H. Cai, X. You, Y. W. Chi, *Analyst* **2015**, *140*, 7468-7486.
[15] Y. Xu, J. Liu, C. Gao, E. Wang, *Electrochem. Commun.* **2014**, *48*, 151-154.
[16] M. Amelia, C. Lincheneau, S. Silvi, A. Credi, *Chem. Soc. Rev.* **2012**, *41*, 5728-5743.
[17] A. Franceschetti, A. Zunger, *Phys. Rev. B* **2000**, *62*, 2614-2623.
[18] L. E. Brus, *J. Chem. Phys.* **1983**, *79*, 5566-5571.
[19] R. Rossetti, S. Nakahara, L. E. Brus, *J. Chem. Phys.* **1983**, *79*, 1086-1088.
[20] M. Bruchez, M. Moronne, P. Gin, S. Weiss, A. P. Alivisatos, *Science* **1998**, *281*, 2013-2016.
[21] W. C. W. Chan, S. M. Nie, *Science* **1998**, *281*, 2016-2018.
[22] N. Myung, X. M. Lu, K. P. Johnston, A. J. Bard, *Nano Lett.* **2004**, *4*, 183-185.
[23] Z. F. Ding, B. M. Quinn, S. K. Haram, L. E. Pell, B. A. Korgel, A. J. Bard, *Science* **2002**, *296*, 1293-1297.
[24] N. Myung, Z. F. Ding, A. J. Bard, *Nano Lett.* **2002**, *2*, 1315-1319.
[25] N. Myung, Y. Bae, A. J. Bard, *Nano Lett.* **2003**, *3*, 1053-1055.
[26] Y. Bae, N. Myung, A. J. Bard, *Nano Lett.* **2004**, *4*, 1153-1161.
[27] X. Liu, H. Jiang, J. P. Lei, H. X. Ju, *Anal. Chem.* **2007**, *79*, 8055-8060.
[28] P. Bertoncello, R. J. Forster, *Biosens. Bioelectron.* **2009**, *24*, 3191-3200.
[29] P. Bertoncello, A. J. Stewart, L. Dennany, *Anal. Bioanal. Chem.* **2014**, *406*, 5573-5587.

[30] M. Hesari, Z. F. Ding, *J. Electrochem. Soc.* **2016**, *163*, H3116-H3131.
[31] Y. L. Mei, H. S. Wang, Y. F. Li, Z. Y. Pan, W. L. Jia, *Electroanalysis* **2010**, *22*, 155-160.
[32] Y. Wusimanjiang, A. Meyer, L. Lu, W. Miao, *Anal. Bioanal. Chem.* **2016**, *408*, 7049-7057.
[33] S. N. Ding, J. J. Xu, H. Y. Chen, *Chem. Commun.* **2006**, 3631-3633.
[34] P. Bertoncello, *Front. Biosci.* **2011**, *16*, 1084-1108.
[35] S. E. K. Kirschbaum, A. J. Baeumner, *Anal. Bioanal. Chem.* **2015**, *407*, 3911-3926.
[36] Z. Y. Liu, W. J. Qi, G. B. Xu, *Chem. Soc. Rev.* **2015**, *44*, 3117-3142.
[37] K. Muzyka, *Biosens. Bioelectron.* **2014**, *54*, 393-407.
[38] S. Liu, X. Zhang, Y. Yu, G. Zou, *Anal. Chem.* **2014**, *86*, 2784-2788.
[39] R. Russell, A. J. Stewart, L. Dennany, *Anal. Bioanal. Chem.* **2016**, *408*, 7129-7136.
[40] H. Wei, E. Wang, *TrAC, Trends Anal. Chem.* **2008**, *27*, 447-459.
[41] H. Sun, L. Wu, W. Wei, X. Qu, *Materials Today* **2013**, *16*, 433-442.
[42] J. H. Xu, Y. Z. Wang, S. S. Hu, *Microchimica Acta* **2017**, *184*, 1-44.
[43] Z. Guo, T. Hao, S. Du, B. Chen, Z. Wang, X. Li, S. Wang, *Biosens. Bioelectron.* **2013**, *44*, 101-107.
[44] W. Liu, Y. Zhang, S. Ge, X. Song, J. Huang, M. Yan, J. Yu, *Anal. Chim. Acta* **2013**, *770*, 132-139.
[45] H. Zhou, N. Gan, T. Li, Y. Cao, S. Zeng, L. Zheng, Z. Guo, *Anal. Chim. Acta* **2012**, *746*, 107-113.
[46] X. Li, X. Tan, J. Yan, Q. Hu, J. Wu, H. Zhang, X. Chen, *Electrochim.Acta* **2016**, *187*, 433-441.
[47] Q. Wang, M. Chen, H. Zhang, W. Wen, X. Zhang, S. Wang, *Biosens. Bioelectron.* **2016**, *79*, 561-567.
[48] Y. Zhang, W. Dai, F. Liu, L. Li, M. Li, S. Ge, M. Yan, J. Yu, *Anal. Bioanal. Chem.* **2013**, *405*, 4921-4929.
[49] H. R. Zhang, J. J. Xu, H. Y. Chen, *Anal. Chem.* **2013**, *85*, 5321-5325.
[50] X. Zhang, B. Zhang, W. J. Miao, G. Z. Zou, *Anal. Chem.* **2016**, *88*, 5482-5488.
[51] X. Zhang, X. Tan, B. Zhang, W. Miao, G. Zou, *Anal. Chem.* **2016**, *88*, 6947-6953.
[52] J. Zhou, Y. P. He, B. Zhang, Q. L. Sun, G. Z. Zou, *Talanta* **2017**, *165*, 117-121.
[53] L. Li, Y. Chen, Q. Lu, J. Ji, Y. Shen, M. Xu, R. Fei, G. Yang, K. Zhang, J. R. Zhang, J. J. Zhu, *Sci. Rep.* **2013**, *3*, 1529.
[54] K. E. Sapsford, L. Berti, I. L. Medintz, *Angew. Chem. Int. Ed.* **2006**, *45*, 4562-4588.
[55] A. R. Clapp, I. L. Medintz, J. M. Mauro, B. R. Fisher, M. G. Bawendi, H. Mattoussi, *JAm. Chem. Soc.* **2004**, *126*, 301-310.
[56] I. L. Medintz, A. R. Clapp, H. Mattoussi, E. R. Goldman, B. Fisher, J. M. Mauro, *Nat. Mater.* **2003**, *2*, 630-638.
[57] J. R. James, M. I. Oliveira, A. M. Carmo, A. Iaboni, S. J. Davis, *Nat. Methods* **2006**, *3*, 1001-1006.
[58] G. Ulrich, R. Ziessel, A. Harriman, *Angew. Chem. Int. Ed.* **2008**, *47*, 1184-1201.
[59] R. Gill, M. Zayats, I. Willner, *Angew. Chem. Int. Ed.* **2008**, *47*, 7602-7625.
[60] T. Wilson, J. W. Hastings, *Annu. Rev. Cell Dev. Biol.* **1998**, *14*, 197-230.
[61] H. Q. Yao, Y. Zhang, F. Xiao, Z. Y. Xia, J. H. Rao, *Angew. Chem. Int. Ed.* **2007**, *46*, 4346-4349.
[62] P. M. Allen, M. G. Bawendi, *J.Am. Chem.Soc.* **2008**, *130*, 9240-9241.
[63] P. M. Allen, W. H. Liu, V. P. Chauhan, J. Lee, A. Y. Ting, D. Fukumura, R. K. Jain, M. G. Bawendi, *J. Am. Chem. Soc.* **2010**, *132*, 470-471.
[64] R. E. Bailey, S. M. Nie, *J. Am. Chem. Soc.* **2003**, *125*, 7100-7106.
[65] G. X. Liang, L. L. Li, H. Y. Liu, J. R. Zhang, C. Burda, J. J. Zhu, *Chem. Commun.* **2010**, *46*, 2974-2976.
[66] A. M. Derfus, W. C. W. Chan, S. N. Bhatia, *Nano Lett.* **2004**, *4*, 11-18.
[67] C. Kirchner, T. Liedl, S. Kudera, T. Pellegrino, A. M. Javier, H. E. Gaub, S. Stolzle, N. Fertig, W. J. Parak, *Nano Lett.* **2005**, *5*, 331-338.
[68] P. Wu, X. P. Yan, *Chem. Soc. Rev.* **2013**, *42*, 5489-5521.
[69] P. Reiss, M. Protiere, L. Li, *Small* **2009**, *5*, 154-168.
[70] J. Wang, X. Jiang, H. Han, *Biosens. Bioelectron.* **2016**, *82*, 26-31.

[71] Y. P. Dong, T. T. Gao, Y. Zhou, J. J. Zhu, *Anal Chem* **2014**, *86*, 11373-11379.
[72] J. Wang, W. W. Zhao, H. Zhou, J. J. Xu, H. Y. Chen, *Biosens Bioelectron* **2013**, *41*, 615-620.
[73] H. Zhou, Y.-Y. Zhang, J. Liu, J.-J. Xu, H.-Y. Chen, *J. Phys. Chem. C* **2012**, *116*, 17773-17780.
[74] L. Deng, H.-Y. Chen, J.-J. Xu, *Electrochem. Commun.* **2015**, *59*, 56-59.
[75] M. S. Wu, L. J. He, J. J. Xu, H. Y. Chen, *Anal. Chem.* **2014**, *86*, 4559-4565.
[76] D. Wang, L. Guo, R. Huang, B. Qiu, Z. Lin, G. Chen, *Sci. Rep.* **2015**, *5*, 7954.
[77] J. Zhang, Z. Gryczynski, J. R. Lakowicz, *Chem. Phys. Lett.* **2004**, *393*, 483-487.
[78] J. Wang, Y. Shan, W. W. Zhao, J. J. Xu, H. Y. Chen, *Anal. Chem.* **2011**, *83*, 4004-4011.
[79] Y. Shan, J. J. Xu, H. Y. Chen, *Chem. Commun.* **2009**, 905-907.
[80] D. Wang, Y. Li, Z. Lin, B. Qiu, L. Guo, *Anal. Chem.* **2015**, *87*, 5966-5972.
[81] D. F. Wang, L. H. Guo, R. Huang, B. Qiu, Z. Y. Lin, G. N. Chen, *Electrochim. Acta* **2014**, *150*, 123-128.
[82] R. Yang, Y. Liu, H. Ye, B. Qiu, Z. Lin, L. Guo, *Electroanalysis* **2016**, *28*, 1783-1786.
[83] L. H. Zhuang, H. Z. Zuo, Z. Q. Wu, Y. Wang, D. J. Fang, D. C. Jiang, *Anal. Chem.* **2014**, *86*, 11517-11522.
[84] A. Periyakaruppan, R. P. Gandhiraman, M. Meyyappan, J. E. Koehne, *Anal. Chem.* **2013**, *85*, 3858-3863.
[85] A. Gholizadeh, S. Shahrokhian, A. I. Zad, S. Mohajerzadeh, M. Vosoughi, S. Darbari, J. Koohsorkhi, M. Mehran, *Anal. Chem.* **2012**, *84*, 5932-5938.
[86] A. Venkatanarayanan, K. Crowley, E. Lestini, T. E. Keyes, J. F. Rusling, R. J. Forster, *Biosens. Bioelectron.* **2012**, *31*, 233-239.
[87] N. P. Sardesai, K. Kadimisetty, R. Faria, J. F. Rusling, *Anal. Bioanal. Chem.* **2013**, *405*, 3831-3838.
[88] K. Kadimisetty, S. Malla, N. P. Sardesai, A. A. Joshi, R. C. Faria, N. H. Lee, J. F. Rusling, *Anal. Chem.* **2015**, *87*, 4472-4478.
[89] W. J. Miao, J. P. Choi, A. J. Bard,*J.Am. Chem. Soc.* **2002**, *124*, 14478-14485.
[90] V. A. Zamolo, G. Valenti, E. Venturelli, O. Chaloin, M. Marcaccio, S. Boscolo, V. Castagnola, S. Sosa, F. Berti, G. Fontanive, M. Poli, A. Tubaro, A. Bianco, F. Paolucci, M. Prato, *ACS Nano* **2012**, *6*, 7989-7997.
[91] G. Valenti, M. Zangheri, S. E. Sansaloni, M. Mirasoli, A. Penicaud, A. Roda, F. Paolucci, *Chem.-Eur. J.* **2015**, *21*, 12640-12645.
[92] G. F. Xu, X. X. Zeng, S. Y. Lu, H. Dai, L. S. Gong, Y. Y. Lin, Q. P. Wang, Y. J. Tong, G. N. Chen, *Luminescence* **2013**, *28*, 456-460.
[93] R. M. Penner, M. J. Heben, T. L. Longin, N. S. Lewis, *Science* **1990**, *250*, 1118-1121.
[94] C. P. Smith, H. S. White, *Anal. Chem.* **1993**, *65*, 3343-3353.
[95] E. J. F. Dickinson, R. G. Compton, *J. Phys Chem. C* **2009**, *113*, 17585-17589.
[96] D. W. M. Arrigan, *Analyst* **2004**, *129*, 1157-1165.
[97] M. Ongaro, P. Ugo, *Anal. Bioanal. Chem.* **2013**, *405*, 3715-3729.
[98] M. E. Sandison, J. M. Cooper, *Lab. Chip* **2006**, *6*, 1020-1025.
[99] L. M. Moretto, M. Tormen, M. De Leo, A. Carpentiero, P. Ugo, *Nanotechnology* **2011**, *22*, 7.
[100] V. P. Menon, C. R. Martin, *Anal. Chem.* **1995**, *67*, 1920-1928.
[101] P. Ugo, L. M. Moretto, S. Bellomi, V. P. Menon, C. R. Martin, *Anal. Chem.* **1996**, *68*, 4160-4165.
[102] L. M. Moretto, N. Pepe, P. Ugo, *Talanta* **2004**, *62*, 1055-1060.
[103] L. X. Cao, P. S. Yan, K. N. Sun, D. W. Wirk, *Electrochim. Acta* **2008**, *53*, 8144-8148.
[104] A. Mardegan, P. Scopece, F. Lamberti, M. Meneghetti, L. M. Moretto, P. Ugo, *Electroanalysis* **2012**, *24*, 798-806.
[105] A. Chen, M. J. Tsao, J. F. Chuang, C. H. Lin, *Electrochim. Acta* **2013**, *89*, 700-707.
[106] W. S. Baker, R. M. Crooks, *J. Phys. Chem. B* **1998**, *102*, 10041-10046.
[107] B. Brunetti, P. Ugo, L. M. Moretto, C. R. Martin, *J. Electroanal. Chem.* **2000**, *491*, 166-174.
[108] C. Amatore, J. M. Saveant, D. Tessier, *J. Electroanal. Chem.***1983**, *147*, 39-51.

[109] S. P. Mucelli, M. Zamuner, M. Tormen, G. Stanta, P. Ugo, *Biosens. Bioelectron.* **2008**, *23*, 1900-1903.
[110] S. Viswanathan, C. Rani, C. Delerue-Matos, *Anal. Chim. Acta* **2012**, *726*, 79-84.
[111] M. Silvestrini, L. Fruk, P. Ugo, *Biosens. Bioelectron.* **2013**, *40*, 265-270.
[112] M. C. Henstridge, R. G. Compton, *Chem. Rec.* **2012**, *12*, 63-71.
[113] O. Sliusarenko, A. Oleinick, I. Svir, C. Amatore, *ChemElectroChem* **2015**, *2*, 1279-1291.
[114] C. Amatore, C. Pebay, L. Servant, N. Sojic, S. Szunerits, L. Thouin, *ChemPhysChem* **2006**, *7*, 1322-1327.
[115] J. E. Bartelt, S. M. Drew, R. M. Wightman, *J. Electrochem. Soc.* **1992**, *139*, 70-74.
[116] G. C. Fiaccabrino, M. Koudelka-Hep, Y. T. Hsueh, S. D. Collins, R. L. Smith, *Anal. Chem.* **1998**, *70*, 4157-4161.
[117] K.-F. Chow, F. Mavré, J. A. Crooks, B.-Y. Chang, R. M. Crooks, *J. Am. Chem. Soc.* **2009**, *131*, 8364-8365.
[118] K. F. Chow, F. Mavre, J. A. Crooks, B. Y. Chang, R. M. Crooks, *J. Am. Chem. Soc.* **2009**, *131*, 8364-+.
[119] S. E. Fosdick, K. N. Knust, K. Scida, R. M. Crooks, *Angew. Chem-Int. Ed.* **2013**, *52*, 10438-10456.
[120] G. Loget, D. Zigah, L. Bouffier, N. Sojic, A. Kuhn, *Acc. Chem. Res.* **2013**, *46*, 2513-2523.
[121] R. M. Crooks, *ChemElectroChem* **2016**, *3*, 357-359.
[122] C. Warakulwit, T. Nguyen, J. Majimel, M. H. Delville, V. Lapeyre, P. Garrigue, V. Ravaine, J. Limtrakul, A. Kuhn, *Nano Lett.* **2008**, *8*, 500-504.
[123] M. Ongaro, A. Gambirasi, P. Ugo, *ChemElectroChem* **2016**, *3*, 450-456.
[124] Q. F. Zhai, X. W. Zhang, Y. C. Han, J. F. Zhai, J. Li, E. K. Wang, *Anal. Chem.* **2016**, *88*, 945-951.
[125] H. B. Habtamu, M. Sentic, M. Silvestrini, L. De Leo, T. Not, S. Arbault, D. Manojlovic, N. Sojic, P. Ugo, *Anal. Chem.* **2015**, *87*, 12080–12087.
[126] K. Honda, M. Yoshimura, T. N. Rao, A. Fujishima, *J. Phys. Chem. B* **2003**, *107*, 1653-1663.
[127] K. Honda, Y. Yamaguchi, Y. Yamanaka, M. Yoshimatsu, Y. Fukuda, A. Fujishima, *Electrochimica Acta* **2005**, *51*, 588-597.
[128] L. Xiao, I. Streeter, G. G. Wildgoose, R. G. Compton, *Sens. Actuators B.* **2008**, *133*, 118-127.
[129] F. Virgilio, M. Prasciolu, P. Ugo, M. Tormen, *Microelectron. Eng.* **2013**, *111*, 320-324.
[130] M. Sentic, F. Virgilio, A. Zanut, D. Manojlovic, S. Arbault, M. Tormen, N. Sojic, P. Ugo, *Anal. Bioanal. Chem.* **2016**, *408*, 7085-7094.